SIAM J. SCI. COMPUT.
Vol. 40, No. 6, pp. B1541–B1576

MIXED AGGREGATED FINITE ELEMENT METHODS FOR THE UNFITTED DISCRETIZATION OF THE STOKES PROBLEM*

SANTIAGO BADIA†, ALBERTO F. MARTIN‡, AND FRANCESC VERDUGO‡

Abstract. In this work, we consider unfitted finite element methods for the numerical approximation of the Stokes problem. It is well-known that these kinds of methods lead to arbitrarily ill-conditioned systems and poorly approximated fluxes on unfitted interfaces/boundaries. In order to solve these issues, we consider the recently proposed aggregated finite element method, originally motivated for coercive problems. However, the well-posedness of the Stokes problem is far more subtle and relies on a discrete inf-sup condition. We consider mixed finite element methods that satisfy the discrete version of the inf-sup condition for body-fitted meshes and analyze how the discrete inf-sup is affected when considering the unfitted case. We propose different aggregated mixed finite element spaces combined with simple stabilization terms, which can include pressure jumps and/or cell residuals, to fix the potential deficiencies of the aggregated inf-sup. We carry out a complete numerical analysis, which includes stability, optimal a priori error estimates, and condition number bounds that are not affected by the small cut cell problem. For the sake of conciseness, we have restricted the analysis to hexahedral meshes and discontinuous pressure spaces. A thorough numerical experimentation bears out the numerical analysis. The aggregated mixed finite element method is ultimately applied to two problems with nontrivial geometries.

Key words. embedded boundary, unfitted finite elements, Stokes, inf-sup, conditioning

AMS subject classifications. 65N12, 65N15, 65N30

DOI. 10.1137/18M1185624

1. Introduction.

Unfitted finite element (FE) techniques are receiving increasing attention since they are very appealing in many practical situations. Such techniques avoid the generation of *body-fitted* meshes, which is a serious bottleneck in large-scale simulations. They are particularly well-suited to multiphase and multiphysics applications with moving interfaces (e.g., fracture mechanics [1], fluid-structure interaction [2], and free surface flows [3]) and in applications with varying domains (e.g., shape or topology optimization [4], additive manufacturing and three-dimensional (3D) printing [5], and stochastic geometry problems [6]). Unfitted FE methods have been named in different ways. When designed for capturing interfaces, they are usually denoted as the extended FE method [7], whereas they are denoted as *embedded* or *unfitted* methods when the motivation is to simulate a problem using a (usually simple) background mesh (see, e.g., the cutFEM method [8] and the finite cell method [9, 10, 11]).

Although useful, unfitted FE methods have known drawbacks. They pose problems to the numerical integration and the imposition of Dirichlet boundary conditions

*Submitted to the journal's Computational Methods in Science and Engineering section May 4, 2018; accepted for publication (in revised form) October 31, 2018; published electronically December 18, 2018.

http://www.siam.org/journals/sisc/40-6/M118562.html

Funding: This work was partially funded by the European Union under the ExaQUte project within the H2020 Framework Programme (grant agreement 800898). The first author received support from the Catalan Government through the ICREA Acadèmia Research Program. The third author received support from the Secretaria d'Universitats i Recerca of the Catalan Government in the framework of the Beatriu Pinós Program (grant 2016 BP 00145).

†Department of Civil and Environmental Engineering. Universitat Politècnica de Catalunya, Jordi Girona 1-3, Edifici C1, 08034 Barcelona, Spain (sbadia@cimne.upc.edu).

‡CIMNE Centre Internacional de Mètodes Numèrics en Enginyeria, UPC, Esteve Terradas 5, 08860 Castelldefels, Spain (amartin@cimne.upc.edu, fverdugo@cimne.upc.edu).

and lead to ill-conditioned systems [12]. For most of the unfitted FE techniques, the condition number of the discrete linear system depends not only on the characteristic element size of the background mesh but also on the ratios for all cut cells of the total cell volume and the cell volume inside the physical domain, which can be arbitrarily small, leading to the so-called small cut cell problem. Methods based on fictitious material [9] require a penalty term that goes to zero with a power of the mesh size for optimal convergence. Thus, the condition numbers of the resulting linear systems are asymptotically affected by the small cut cell problem. For further details about the convergence behavior of fictitious material methods, see [13]. Preconditioned iterative linear solvers suitable for standard FE methods are not robust for these formulations. Recently, a robust domain decomposition preconditioner able to deal with cut cells has been proposed in [14] for first order methods, but these preconditioners still require some special treatment for the robust direct solution of local-to-subdomain systems. On the other hand, ill-posed degrees of freedom (DOFs) on cut cells can lead to poorly approximated fluxes on unfitted boundaries/interfaces, which is especially critical for interface-coupled problems like fluid-structure interaction.

The authors have recently proposed in [15] an unfitted FE formulation, referred to as the aggregated finite element method (agFEM), which fixes the small cut cell problems for elliptic partial differential equations (PDEs). This novel method relies on the so-called aggregated finite element (agFE) spaces, grounded on cell aggregation techniques and judiciously chosen linear constraints for conflictive DOFs with respect to interior ones. This approach can be applied to grad-conforming (globally continuous) spaces and discontinuous FE spaces of arbitrary order. The agFEM leads to a well-posed Galerkin formulation of elliptic problems, viz., no stabilization terms are needed and the method is thus consistent and does not introduce artificial diffusion. Furthermore, the resulting linear systems have condition numbers that scale only with the element size of the background mesh in the same way as in standard FE methods for body-fitted meshes. These methods have been implemented in `FEMPAR`, a large-scale FE software package [16, 17].

Among other existing approaches, the most salient one is the *ghost penalty* formulation used in the CutFEM method [8, 18]. The most widely used version of this method requires computing high order derivatives on facets for high order FEs, which are not at our disposal in general FE codes and are expensive to compute, certainly complicating the implementation of the methods and harming code performance. Other versions of the ghost penalty method that do not require the computation of high order derivatives but rely on some macroelement mesh structure have been proposed for some problems (see, e.g., [19] for the Poisson equation and [20, 21] for the time-dependent convection-diffusion equation on moving domains). For B-spline approximations, one can consider the so-called extension or extrapolation techniques (see, e.g., [22, 23, 24]). These works are close to the agFEM [15] in the sense that the problematic DOFs associated with B-splines with small support inside the physical domain are eliminated by constraining them as a linear combination of *well-posed* DOFs. Such aggregation approaches are not new in discontinuous Galerkin (DG) methods (see, e.g., [25, 26, 27]), for which the situation is much easier, since no conformity must be kept. In fact, some aggregation techniques in DG [25, 26, 27] can be cast as discontinuous agFEMs.

The use of mixed FE methods on unfitted meshes has been explored in previous works. The combination of ghost penalty stabilization and inf-sup stable elements for the unfitted FE approximation of the Stokes problem was originally addressed in [28] for triangular meshes in two dimensions. The analysis therein relies on the

continuous inf-sup condition on the interior domain, viz., the union of interior cells (not intersecting the boundary), in order to prove pressure stability in interior cells, whereas cut cell pressure stability relies on ghost penalty stabilization. The extension of this work to interface Stokes problems for the MINI element has been proposed in [29] (see also [30] for a similar strategy). The analyses in [28, 29, 30] rely on the assumption that the discrete inf-sup constant is bounded away from zero uniformly in h. This uniform stability is not trivial, and it has only been proved so far for triangular/tetrahedral meshes and some mixed FEs (see [31]). As an alternative to mixed FE methods, globally stabilized residual-based and pressure jump first order schemes combined with ghost penalty stabilization have been used in [32]. Global residual-based stabilization has also been used in [23, 24] for B-spline approximations.

In this work, we propose to combine the agFEM approach, which fixes the small cut cell problem for the numerical approximation of elliptic PDEs, with mixed FE spaces. Unsurprisingly, the development of mixed agFE spaces that satisfy a discrete version of the inf-sup condition is not straightforward. The discrete inf-sup condition requires a perfect balance of the velocity and pressure spaces, whereas the boundary-cell intersections can be arbitrary, leading to a large set of possible cell aggregates geometries. We consider hexahedral meshes and arbitrary order mixed FE spaces with discontinuous pressures and analyze the potential deficiencies of the *unfitted* inf-sup in terms of a set of *improper* aggregates and interfaces that will require additional stabilization.[1] An abstract stability analysis under some assumptions about such stabilization allows us to define effective stabilization terms. We propose two algorithms. The first one combines a standard aggregated tensor-product Lagrangian FE with interior residual-based and pressure jump face stabilization on improper aggregates and facets, respectively. The second one makes use of an agFE space in terms of a serendipity-based extension of tensor-product Lagrangian FEs combined with pressure jump stabilization on improper facets. The resulting schemes can be used in quadrilateral/hexahedral meshes, the order of approximation can be selected by the user, the algorithm does not require us to compute (higher than order one) derivatives on cell boundaries (unlike ghost penalty/cutFEM approaches), and it involves minimal stabilization and consequently artificial diffusion (e.g., only pressure jump stabilization on a very small subset of facets *close* to the interface). A complete numerical analysis shows the uniform stability (that does not rely on the potentially ill inf-sup condition on the union of interior cells), optimal a priori error estimates, and condition number bounds with respect to the mesh size and cell boundary intersection. Another remarkable feature of our approach is that it exposes a high degree of message-passing parallelism in the assembly process, and thus it is suitable for the development of a highly scalable parallel unfitted FE framework on distributed memory computers, so far still missing in the literature. In fact, a highly scalable parallel implementation of agFEM on nonconforming h-adaptive octree meshes, grounded on `p4est` for efficient octree handling [33], is under development in `FEMPAR` [16, 17]. Apart from their ability to control geometry approximation errors by local adaptation in regions of high geometric variability, octree meshes can be very efficiently generated, refined and coarsened, partitioned, and 2:1 balanced on hundreds of thousands of processors [33], the latter being the main reason why we favor this sort of mesh in our approach.

The outline of this work is as follows. In section 2, we introduce the Stokes problem and, in section 3, a brief introduction to FE spaces, and some notation fol-

[1] In any case, these ideas could be extended to tetrahedral meshes and other mixed FE spaces.

lows. Section 4 is devoted to the definition of agFE spaces and their mathematical properties. A discrete agFEM for the approximation of the Stokes problem is proposed in section 5, in which the stabilization terms are not defined yet. Section 6 is devoted to a complete numerical analysis of mixed agFEMs. More specifically, in section 6.1, we perform an abstract stability analysis under some assumptions over the mixed agFE space and the stabilization terms. Two different algorithms that satisfy these assumptions are proposed in sections 6.2 and 6.3. A priori error estimates and condition number bounds that are independent of the cut cell intersection with the boundary are proved in sections 6.4 and 6.5, respectively. A complete set of numerical experiments can be found in section 7. To close this work, some conclusions are drawn in section 8.

2. Problem statement. Let us consider an open and bounded physical domain $\Omega \subset \mathbb{R}^d$ (where $d = 2, 3$ is the physical space dimension) with Lipschitz boundary Γ, occupied by a viscous fluid. We consider Dirichlet boundary conditions on Γ for brevity in the exposition; the introduction of Neumann boundary conditions is straightforward. The Stokes problem, after scaling the pressure with the inverse of the diffusion coefficient, reads as follows: find the velocity field $\boldsymbol{u} : \Omega \to \mathbb{R}^d$ and the pressure field $p : \Omega \to \mathbb{R}$ such that

$$-\Delta \boldsymbol{u} + \boldsymbol{\nabla} p = \boldsymbol{f} \quad \text{in } \Omega, \qquad \boldsymbol{\nabla} \cdot \boldsymbol{u} = 0 \quad \text{in } \Omega, \qquad \boldsymbol{u} = \boldsymbol{g} \quad \text{on } \Gamma, \tag{1}$$

where $\boldsymbol{f}$ is the body force and $\boldsymbol{g}$ is the prescribed Dirichlet data, which must satisfy $\int_\Gamma \boldsymbol{g} \cdot \boldsymbol{n} = 0$, where $\boldsymbol{n}$ stands for the outward normal. In order to uniquely determine the pressure, we additionally enforce that $\int_\Omega p = 0$.

We use standard notation for Sobolev spaces (see [34]). In particular, the $L^2(\omega)$ scalar product will be denoted by $(\cdot, \cdot)_\omega$ for some $\omega \subset \mathbb{R}^d$. Making abuse of notation, we represent the $H^1(\omega)$ duality pairing the same way. $L^2_0(\omega)$ is the subspace of functions in $L^2(\omega)$ with zero mean value. For a Sobolev space X, we denote its norm by $\|\cdot\|_X$. In particular, the $L^2(\omega)$ norm is denoted by $\|\cdot\|_\omega$ and the $H^1(\omega)$ norm as $\|\cdot\|_{1,\omega}$. The seminorm on the Sobolev space $W^{k,p}(\omega)$ is denoted by $|\cdot|_{W^{k,p}(\omega)}$, or simply $|\cdot|_{1,\omega}$ for $H^1(\omega)$. Given a function $g \in H^{\frac{1}{2}}(\partial\omega)$, the subspace of functions in $H^1(\omega)$ with trace equal to g is represented with $H^1_g(\omega)$. Vector-valued Sobolev spaces are represented with boldface letters.

Let us assume that $\boldsymbol{f} \in \boldsymbol{L}^2(\Omega)$ and $\boldsymbol{g} \in \boldsymbol{H}^{\frac{1}{2}}(\Gamma)$. The weak form of the Stokes problem (1) reads as follows: find $(\boldsymbol{u}, p) \in \boldsymbol{H}^1_{\boldsymbol{g}}(\Omega) \times L^2_0(\Omega)$ such that

$$(\boldsymbol{\nabla} \boldsymbol{u}, \boldsymbol{\nabla} \boldsymbol{v})_\Omega - (p, \boldsymbol{\nabla} \cdot \boldsymbol{v})_\Omega - (q, \boldsymbol{\nabla} \cdot \boldsymbol{u})_\Omega = (\boldsymbol{f}, \boldsymbol{v})_\Omega \tag{2}$$

for any $(\boldsymbol{v}, q) \in \boldsymbol{H}^1_{\boldsymbol{0}}(\Omega) \times L^2_0(\Omega)$. The well-posedness of this linear problem relies on the fact that the divergence operator on $\boldsymbol{H}^1_{\boldsymbol{0}}(\Omega)$ is surjective in $L^2_0(\Omega)$. There exists a constant β that depends on Ω such that (see, e.g., [35])

$$\inf_{p \in L^2_0(\Omega)} \sup_{\boldsymbol{v} \in \boldsymbol{H}^1_{\boldsymbol{0}}(\Omega)} \frac{(p, \boldsymbol{\nabla} \cdot \boldsymbol{v})_\Omega}{\|p\|_\Omega \|\boldsymbol{v}\|_{1,\Omega}} \geq \beta > 0. \tag{3}$$

In the following exposition, we consider the numerical approximation of this problem by using FE methods. In particular, we are interested in the discretization of the Stokes problem when using unfitted FE methods, i.e., the mesh is not fitted to Ω.

3. FE spaces. Let us consider an open polyhedral domain ω and its partition $\mathcal{K}_h(\omega)$ into a set of cells. We may consider the case in which all cells are hexahedra/quadrilaterals (hex mesh) or all cells are tetrahedra/triangles (tet mesh). At any

cell $K \in \mathcal{K}_h(\omega)$, we define the local FE spaces as follows. Using the abstract definition of Ciarlet, an FE is represented by the triplet $\{K, \mathcal{V}, \Sigma\}$, where K is a compact, connected, Lipschitz subset of $\mathbb{R}^d$, $\mathcal{V}$ is a vector space of functions, and Σ is a set of linear functionals that form a basis for the dual space $\mathcal{V}'$. The elements of Σ are the so-called DOFs of the FE; we denote the number of DOFs as n_Σ. The DOFs can be written as σ^a for $a \in \mathcal{N}_\Sigma \doteq \{1, \dots, n_\Sigma\}$. We can also define the basis $\{\phi^a\}_{a \in \mathcal{N}_\Sigma}$ for $\mathcal{V}$ such that $\sigma^a(\phi^b) = \delta_{ab}$ for $a, b \in \mathcal{N}_\Sigma$. These functions are the so-called shape functions of the FE, and there is a one-to-one mapping between shape functions and DOFs.

In this work, we consider three different concretizations of the vector space $\mathcal{V}$: (1) the space $\mathcal{P}_q(K)$ of polynomials of degree less than or equal to q; (2) the space $\mathcal{Q}_q(K)$ of polynomials of degree less than or equal to q with respect to each reference space coordinate; (3) the space $\breve{\mathcal{Q}}_q(K)$ of polynomials of superlinear degree less than or equal to q (see [36] for more details). $\breve{\mathcal{Q}}_q(K)$ on hex meshes leads to the *serendipity* FE. For the sake of simplicity, we assume that all cells in the mesh have the same topology and (for a given field) the same polynomial order.[2]

In order to build globally continuous FE spaces, we denote by $\mathcal{N}(K)$ the set of n_Σ Lagrangian nodes of order q of cell K for $\mathcal{P}_q(K)$ in tets and $\mathcal{Q}_q(K)$ in hexs. The set of nodal values, i.e., $\sigma^a(v) \doteq v(\boldsymbol{x}^a)$ for $a \in \mathcal{N}(K)$, is a basis for the dual space $\mathcal{V}'$. By definition, it holds that $\phi^a(\boldsymbol{x}^b) = \delta_{ab}$, where $\boldsymbol{x}^b$ are the space coordinates of node b in the corresponding set of nodes. Next, we assume that there is a local-to-global DOF map such that the resulting global space is $\mathcal{C}^0$ continuous. It leads to the following $\mathcal{C}^0(\omega)$ global FE spaces: (1) the space $\mathcal{P}_{q,h}(\omega)$ of functions such that its cell restriction belongs to $\mathcal{P}_q(K)$ for a tet mesh; (2) the space $\mathcal{Q}_{q,h}(\omega)$ (resp., $\breve{\mathcal{Q}}_{q,h}(\omega)$) of functions such that its cell restriction belongs to $\mathcal{Q}_q(K)$ (resp., $\breve{\mathcal{Q}}_q(K)$) for a hex mesh. We note that for discontinuous FE spaces, the definition of DOF is flexible, since no intercell continuity must be enforced. We will make use of the global space $\mathcal{P}^-_{q,h}(\omega)$ of piecewise discontinuous functions that belong to $\mathcal{P}_q(K)$, for an *arbitrary* cell topology. The spaces of vector-valued functions with components in these spaces are represented with boldface letters.

Given a function v, we define the *local interpolator* for nodal Lagrangian FEs as

$$\pi_K^I(v) \doteq \sum_{a \in \mathcal{N}(K)} \sigma^a(v)\phi^a = \sum_{a \in \mathcal{N}(K)} v(\boldsymbol{x}^a)\phi^a, \qquad K \in \mathcal{K}_h(\omega). \tag{4}$$

It is easy to check that the interpolation operator is in fact a projection. The global interpolator $\pi_h^I(\cdot)$ is defined as the sum over the cells of the corresponding local interpolators, i.e., $\pi_h^I(v) = \sum_{K \in \mathcal{K}_h(\omega)} \pi_K^I(v)$.

4. Aggregated finite element spaces. In this section, we define agFE spaces. We refer to [15] for more details. First, we introduce some geometrical concepts related to the use of embedded boundary methods, the cell aggregation algorithm, and the map between vertices, edges, and faces (VEFs) on cut cells and aggregates. Next, we use the geometrical aggregation to define agFE spaces on unfitted meshes. Finally, we provide some trace and inverse inequalities, together with approximability

[2]The polynomial spaces are defined in the physical space cell, instead of relying on a reference cell and a map from the reference to the physical space. Both approaches are equivalent for affine maps, whereas the second one is more appealing due to lower computational cost. The convergence properties of serendipity FEs are deteriorated if the map is not affine [37]. Fortunately, the equivalence holds for the Cartesian hex meshes below.

properties that will be used in the following sections to analyze the stability and to obtain a priori error estimates. In the following, we assume that hex meshes are being used. In practice, we are interested in Cartesian hex meshes, where all the cells can be represented as the scaling of a d-cube. This restriction simplifies implementation issues, since polynomial bases in the physical space can be obtained as the mapped reference cell polynomial bases, a fact that does not hold for general (first-order) hex meshes. However, agFE spaces can readily be obtained for tet meshes using the ideas below.

4.1. Embedded boundary setup and cell aggregation. As usual for embedded boundary methods, we consider an *artificial* domain Ω_{art} with a simple shape that can easily be meshed using a conforming Cartesian grid $\mathcal{K}_h^{\text{art}} \doteq \mathcal{K}_h(\Omega_{\text{art}})$ of characteristic size h that includes the *physical* domain $\Omega \subset \Omega_{\text{art}}$ (see Figure 1(a)). In the numerical analysis, no geometrical error will be considered. In our practical implementation, the domain boundary is implicitly defined as the zero level-set of a given scalar function ψ^{ls}, i.e., $\Gamma \doteq \{\boldsymbol{x} \in \mathbb{R}^d : \psi^{\text{ls}}(\boldsymbol{x}) = 0\}$. It leads to an approximation Ω_h of Ω, e.g., using a marching cubes–like algorithm, which also leads to an approximated boundary Γ_h. We will omit the subscript for the sake of conciseness in the notation, unless the distinction is important.

Let us define the quantity $\eta_K \doteq \frac{|K \cap \Omega|}{|K|}$ and a parameter $\eta_0 \in (0, 1]$. Cells in $\mathcal{K}_h^{\text{art}}$ can be classified as follows: a cell $K \in \mathcal{K}_h^{\text{art}}$ such that $\eta_K \geq \eta_0$ is an *interior cell*;[3] if $K \cap \Omega = \emptyset$, K is an *external cell*; otherwise, K is a *cut cell* (see Figure 1(b)). The set of interior (resp., external and cut) cells is represented with $\mathcal{K}_h^{\text{in}}$ and its union $\Omega_{\text{in}} \subset \Omega$ (resp., $(\mathcal{K}_h^{\text{ext}}, \Omega_{\text{ext}})$ and $(\mathcal{K}_h^{\text{cut}}, \Omega_{\text{cut}})$). Furthermore, we define the set of *active cells* as $\mathcal{K}_h \doteq \mathcal{K}_h^{\text{in}} \cup \mathcal{K}_h^{\text{cut}}$ and its union Ω_{act}. We assume that the background mesh is *quasi-uniform* (see, e.g., [38, p. 107]) to reduce technicalities, and we define a characteristic mesh size h.

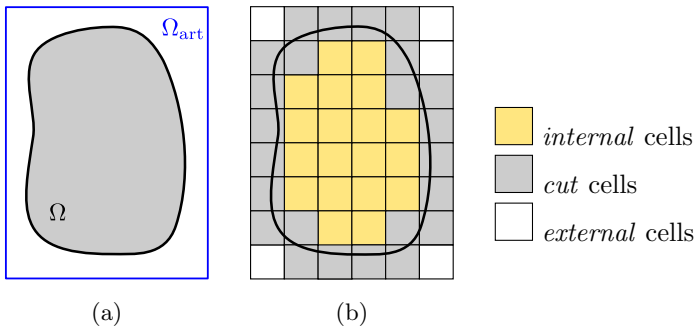

FIG. 1. *Embedded boundary setup.*

We can also consider a partition of Ω into nonoverlapping cell aggregates. Each aggregate is composed of several cut cells and *only* one interior cell. Besides, the cells in an aggregate are connected, i.e., an aggregate cannot span multiple disjoint domains. Such partition can be computed using the strategy described in Algorithm 4.1 below.

[3]For $\eta_0 = 1$, *interior* cells are cells $K \subset \Omega$. However, we can weaken the definition by taking lower values of η_0, considering also as *interior* cells the ones that have a large enough portion in the interior.

ALGORITHM 4.1 (cell aggregation algorithm).

1. *Mark all interior cells as touched and all cut cells as untouched.*
2. *For each untouched cell, if there is at least one touched cell connected to it through a facet F such that $F \cap \Omega \neq \emptyset$, we aggregate the cell to the touched cell belonging to the aggregate containing the closest interior cell. If more than one touched cell fulfills this requirement, we choose one arbitrarily, e.g., the cell connected via the facet with more area inside the physical domain, or the one with the smaller global label.*
3. *Mark as touched all the cells aggregated in step* 2.
4. *Repeat steps* 2 *and* 3 *until all cells are aggregated.*

Figure 2 shows an illustration of each step in Algorithm 4.1 for $\eta_0 = 1$. The black thin lines represent the boundaries of the aggregates. Note that from step 1 to step 2, some of the lines between adjacent cells are removed, meaning that the two adjacent cells have been merged in the same aggregate. The aggregation schemes can be easily applied to arbitrary spatial dimensions.

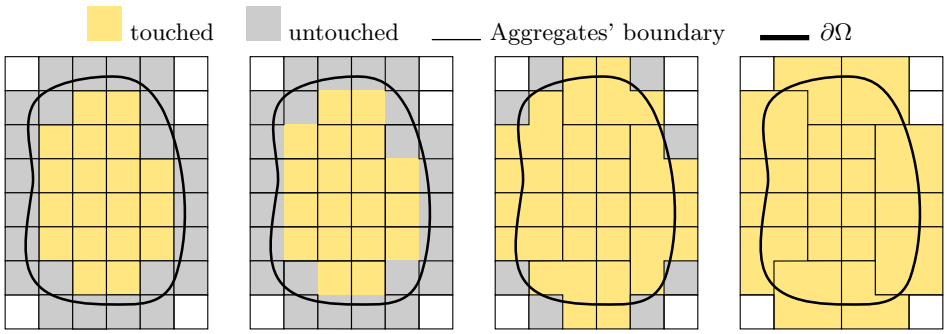

(a) Step 1. (b) Step 2. (c) Step 3. (d) Step 4.

FIG. 2. *Illustration of the cell aggregation scheme defined in Algorithm* 4.1 *for $\eta_0 = 1$. We note that the definition of an aggregate in* (5) *is such that it only considers the part of the aggregated cells inside Ω as this simplifies the notation in the numerical analysis.*

In the forthcoming sections, we need an upper bound of the size of the aggregates generated with Algorithm 4.1 in terms of the cell mesh size h, i.e., the characteristic size of an aggregate is bounded by γh for some γ independent of h and the cut cell intersection with the boundary. For a given mesh, the constant γ can be bounded using the following result taken from [15, Lemma 2.2].

LEMMA 4.2. *Assume that from any cut cell $K_0 \in \mathcal{K}_h^{\text{act}}$ there is a cell path $\{K_0, K_1, \ldots, K_n\}$ that satisfies the following:* (1) *two consecutive cells share a facet F such that $F \cap \Omega \neq \emptyset$;* (2) *$K_n$ is an interior cell; and* (3) *$n \leq n_{\max}$, where $n_{\max}$ is a fixed integer. Then, the constant γ is at most $2n_{\max} + 1$.*

The lemma states that the aggregate size is bounded in terms of $n_{\max}$, i.e., the number of cells that need to be traversed via facets for connecting a cut cell with an interior one. Note that large values of $n_{\max}$ can only appear when dealing with underresolved geometrical details. Thus, finer meshes contribute to decrease $n_{\max}$ and, in turn, the aggregate size. The numerical results in [15, section 6.3] show that γ tends to $\gamma = 2$ in two dimensions and $\gamma = 3$ in three dimensions for some practical cases. However, for complex geometries, local mesh adaptation could be required to capture small geometrical details and reduce the aggregate size.

Algorithm 4.1 leads to another partition $\mathcal{T}_h$ into aggregates, where an aggregate is defined in terms of a set of cells as

$$A \doteq \tilde{A} \cap \Omega, \quad \tilde{A} \doteq \{\cup_{i=0}^{n_A} K_i : \ K_i \in \mathcal{K}_h\}, \tag{5}$$

where (without loss of generality) $K_0 \in \mathcal{K}_h^{\text{in}}$ is the owner interior cell, also represented with $\mathcal{O}(A)$. Thus, $A \in \mathcal{T}_h$ is *trimmed* by the boundary and $\tilde{A}$ is its corresponding *untrimmed* aggregate. In the following, trimmed aggregates will just be referred to as aggregates. By construction of Algorithm 4.1, it holds that (1) $n_A \geq 0$; (2) interior cells that have no aggregated cut cells ($n_A = 0$) remain the same; (3) there is only one interior cell per aggregate, i.e., $K_i \not\subset \Omega$ for $i > 0$; (4) every cut cell belongs to one and only one aggregate.

For an interior/cut cell $K \in \mathcal{K}_h$, we define its owner (interior) cell $\mathcal{O}(K)$ as the owner $\mathcal{O}(A)$ of the only aggregate $A \in \mathcal{T}_h$ that contains the cell, i.e., $K \cup A$ has nonzero measure in dimension d. Thus, the owner of an interior cell is the cell itself.

We can also construct a map that, given an *outer* VEF, i.e., a VEF that belongs to at least one cut cell in $\mathcal{K}_h^{\text{cut}}$ but does not belong to any interior cell in $\mathcal{K}_h^{\text{in}}$, provides its aggregate owner among all the aggregates that contain it (see Figure 3). This map can be arbitrarily built, e.g., we can consider the *smallest* aggregate that contains the VEF. The map between the outer VEF b and the interior cell owner is *also* represented with $\mathcal{O}(b)$.[4]

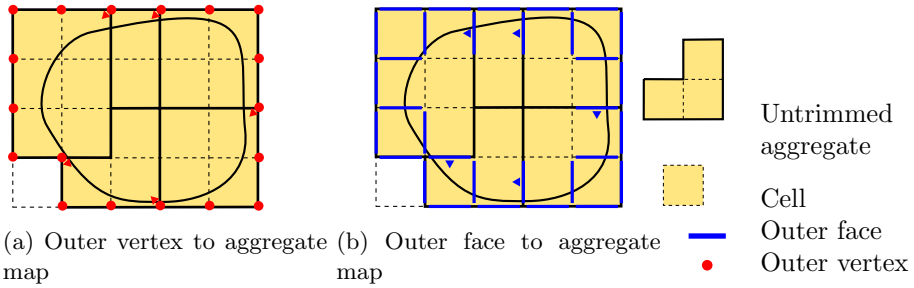

(a) Outer vertex to aggregate map (b) Outer face to aggregate map

FIG. 3. *Map from outer facets and vertex to aggregate owner. The small pointers denote the aggregate owner. Pointers are not used for vertex and facets belonging to only one aggregate since the owner is obvious. Aggregates in* (a) *and* (b) *are the same, but the aggregate bounds are clearer in* (a).

4.2. Aggregated finite element spaces. Our goal is to define FE spaces using the cell aggregates introduced above, in order to end up with unfitted FE spaces on the domain Ω, with optimal approximability properties not affected by the small cut cell problem. The goal of this section is to start with a pair of inf-sub stable FE spaces (i.e., velocity-pressure pairs of FE spaces that satisfy a discrete version of the inf-sup condition on body-fitted meshes) and to end up with an *aggregated* version of this FE pair (which will not be affected by the small cut cell problem). The process of defining the aggregated version of a given FE space can be introduced systematically for different types of interpolations. For the sake of simplicity, we present the method for a generic scalar-valued field. The technique will be eventually applied to the FE

[4] After the cell aggregation and the VEF owner definition, we have defined a map $\mathcal{O}(\cdot)$ that, given any outer VEF or cut cell, provides its owner (interior) cell.

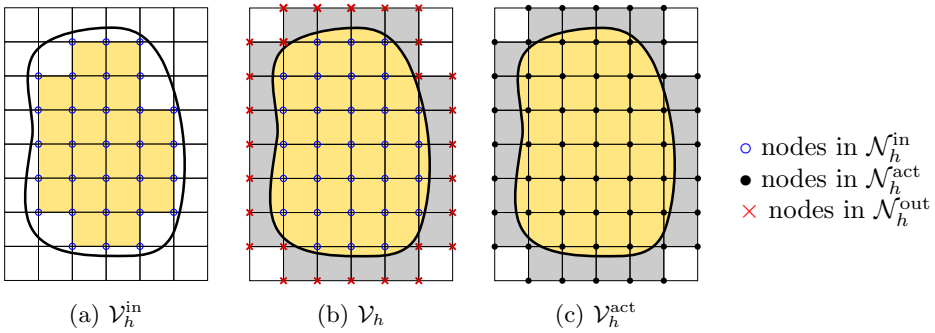

FIG. 4. *FE spaces.*

space for the pressure field, and to each component of the FE space for the velocity field (which are a scalar FE spaces).

Let us represent with $\mathcal{V}_h(\omega)$ a generic global (continuous or discontinuous) Lagrangian FE space, i.e., it can be $\mathcal{Q}_{q,h}$ for hex meshes and $\mathcal{P}_{q,h}$ for tet meshes, for an arbitrary order q. We introduce the *active* FE space associated with the active portion of the background mesh $\mathcal{V}_h^{\text{act}} \doteq \mathcal{V}_h(\mathcal{K}_h^{\text{act}})$ and the *interior* FE space $\mathcal{V}_h^{\text{in}} \doteq \mathcal{V}_h(\mathcal{K}_h^{\text{in}})$. The active FE space $\mathcal{V}_h^{\text{act}}$ (see Figure 4(c)) is the functional space typically used in unfitted FE methods (see, e.g., [14, 12, 9]). It is well-known that $\mathcal{V}_h^{\text{act}}$ leads to arbitrary ill-conditioned systems when integrating the FE weak form on the physical domain Ω only (if no stabilization technique is used to remedy it). It is obvious that the interior FE space $\mathcal{V}_h^{\text{in}}$ (see Figure 4(a)) is not affected by this problem, but it is not usable since it is not defined on Ω.

Herein, we propose an alternative agFE space $\mathcal{V}_h$ that is defined on Ω but does not present the ill-conditioning issues related to $\mathcal{V}_h^{\text{act}}$. To this end, we can define the set of nodes of $\mathcal{V}_h^{\text{in}}$ and $\mathcal{V}_h^{\text{act}}$ as $\mathcal{N}_h^{\text{in}}$ and $\mathcal{N}_h^{\text{act}}$, respectively (see Figure 4). We define the set of *outer* nodes as $\mathcal{N}_h^{\text{out}} \doteq \mathcal{N}_h^{\text{act}} \backslash \mathcal{N}_h^{\text{in}}$ (e.g., the nodes that belong to outer VEFs in Figure 3). The outer nodes are the ones that can lead to conditioning problems due to the small cut cell problem (see, e.g., [12]). The space of global shape functions of $\mathcal{V}_h^{\text{in}}$ and $\mathcal{V}_h^{\text{act}}$ can be represented as $\{\phi^b : b \in \mathcal{N}_h^{\text{in}}\}$ and $\{\phi^b : b \in \mathcal{N}_h^{\text{act}}\}$, respectively. Any function $u_h \in \mathcal{V}_h^{\text{in}}$ can be written as $u_h = \sum_{a \in \mathcal{N}_h^{\text{in}}} u_h^a \phi^a$, and analogously for functions in $\mathcal{V}_h^{\text{act}}$. The space $\mathcal{V}_h$ is defined taking as the starting point $\mathcal{V}_h^{\text{act}}$ and adding judiciously defined constraints for the nodes in $\mathcal{N}_h^{\text{out}}$.

In order to define $\mathcal{V}_h$, we observe that, in nodal Lagrangian FE spaces, there is a one-to-one map between DOFs and nodes (points) of the FE mesh. For globally continuous FE spaces, we can define the owner VEF of an outer node $b \in \mathcal{N}_h^{\text{out}}$, denoted as $\mathcal{O}^{\text{vef}}(b)$, as the lowest-dimensional VEF that contains the node b. As a result, the composition of the outer-VEF-to-cell-owner map $\mathcal{O}(\cdot)$ with the outer-DOF-to-vef-owner map $\mathcal{O}^{\text{vef}}(\cdot)$ leads to an outer-DOF-to-cell-owner map, namely, $\mathcal{O} \circ \mathcal{O}^{\text{vef}}(\cdot)$. Abusing notation, we also denote this map as $\mathcal{O}(b)$ for an outer DOF b. For discontinuous FE spaces, all the DOFs belong to the cell itself, since no continuity must be enforced. Thus, the DOFs owner and outer-DOFs-to-cell maps are trivial once defined the cell aggregation. Since no continuity must be enforced among cells, the definition of DOFs is very flexible.

Given a function $v_h \in \mathcal{V}_h^{\text{in}}$ and a cell $K \in \mathcal{K}_h^{\text{in}}$, we define the unique polynomial $\xi_h^K(v_h) : \mathbb{R}^d \to \mathbb{R}$ such that its restriction to the cell K coincides with the FE function,

i.e., $v_h(\boldsymbol{x}) = \xi_h^K(v_h)(\boldsymbol{x})$, $\boldsymbol{x} \in K$. With these ingredients, we define $\mathcal{V}_h \subset \mathcal{V}_h^{\text{act}}$ as the subset of functions in $\mathcal{V}_h^{\text{act}}$ such that, for any DOF $a \in \mathcal{N}_h^{\text{out}}$,

$$v_h^a = \sigma^a(\xi_h^{\mathcal{O}(a)}(v_h)) = \sum_{b \in \mathcal{N}(\mathcal{O}(a))} \sigma^a(\xi_h^{\mathcal{O}(a)}(\phi^b))\sigma^b(v_h). \tag{6}$$

By construction, functions in $\mathcal{V}_h$ are uniquely determined by the DOFs of $\mathcal{V}_h^{\text{in}}$. Thus, we can define the extension operator $\mathcal{E}_h : \mathcal{V}_h^{\text{in}} \to \mathcal{V}_h \subset \mathcal{V}_h^{\text{act}}$ such that given $u_h \in \mathcal{V}_h^{\text{in}}$ provides the FE function $\mathcal{E}_h(u_h) \in \mathcal{V}_h^{\text{act}}$ with outer nodal values computed as in (6). See Figure 5 for an illustration of the extension operator $\mathcal{E}_h(\cdot)$. Thus, the agFE space is the range of this operator, i.e., $\mathcal{V}_h \doteq \mathcal{E}_h(\mathcal{V}_h^{\text{in}}) \subset \mathcal{V}_h^{\text{act}}$. If functions in $\mathcal{V}_h^{\text{act}}$ are $\mathcal{C}^0$ continuous, since $\mathcal{V}_h \subset \mathcal{V}_h^{\text{act}}$, then functions in $\mathcal{V}_h$ are also $\mathcal{C}^0$ continuous. We note that (6) makes sense for continuous and discontinuous spaces, and, e.g., both tensor-product and serendipity spaces for hex meshes and Lagrangian FEs for tet meshes. In any case, the definition in (6) is general and can be used for spaces with DOFs that are not nodal evaluations.

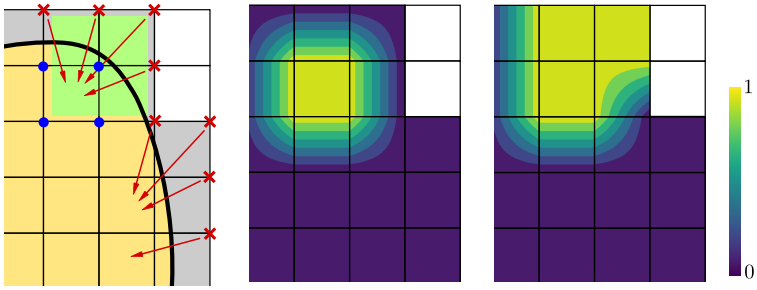

(a) DOFs owners (b) $v_h \in \mathcal{V}_h^{\text{in}}$ (c) $\mathcal{E}(v_h) \in \mathcal{V}_h$

FIG. 5. *Illustration of the extension operator $\mathcal{E}_h(\cdot)$. The red arrows represent the exterior DOF to interior cell map $\mathcal{O}(\cdot)$. Function v_h is equal to* 1 *at the DOFs associated with the root cell of the aggregate displayed in* (a) *and equal to* 0 *elsewhere. By formula* (6)*, the extended function $\mathcal{E}_h(v_h)$ is also* 1 *at the exterior DOFs whose cell owner is the root cell of the aggregate in* (a)*. Note that not all DOFs in an aggregate need to share the same cell owner.*

4.2.1. Nodal Lagrangian aggregated finite element spaces. In particular, for nodal-based Lagrangian FE spaces (which include tensor-product $\mathcal{Q}_{q,h}(\mathcal{K}_h)$ and serendipity spaces $\breve{\mathcal{Q}}_{q,h}(\mathcal{K}_h)$ for hex meshes and $\mathcal{P}_{q,h}(\mathcal{K}_h)$ for tet meshes), the previous expression is reduced to

$$v_h(\boldsymbol{x}^a) = \sum_{b \in \mathcal{N}(\mathcal{O}(a))} v_h(\boldsymbol{x}^b)\phi^b(\boldsymbol{x}^a). \tag{7}$$

The computation of the constraint is straightforward and simply involves evaluating the shape function polynomials of a cell in a set of points that do not belong to the cell, viz., the nodes of an aggregated cut cell. The definition of DOF ownership is simple: the VEF or cell that contains the node related to the DOF with minimum dimension, which is uniquely defined.

4.2.2. Discontinuous aggregated finite element spaces. Let us comment on discontinuous FE spaces, e.g., $\mathcal{P}_{q,h}^-(\mathcal{K}_h)$ on hex meshes. It is easy to check that for discontinuous spaces, the agFE space can be analogously defined as

$$\mathcal{V}_h = \{v : v|_A \in \mathcal{P}_q^-(A) \text{ for any } A \in \mathcal{T}_h\}. \tag{8}$$

The equivalence between the definition based on (6) and the one in (8) is straightforward. The use of aggregation techniques within DG methods has already been used, e.g., in [39, 27].

4.2.3. Aggregated finite elements with serendipity extension. Up to now, we have assumed that the constraints for the extension operator were computed using the same shape functions as the ones of the local FE space in the owner interior cell (see (6)). Here, we consider a more general case in which these two shape functions bases (and the corresponding spanned spaces) can differ. In particular, we are interested in using a tensor-product Lagrangian space at all cells in a hex mesh, but to compute the constraints through the corresponding serendipity basis (preserving the order of approximation). As we will see later on, it does not affect accuracy and has positive properties when considering stable mixed agFE spaces (see section 6.3).

Let us introduce some notation, in order to distinguish between tensor-product and serendipity FE spaces. For serendipity FEs and hex meshes, i.e., $\breve{\mathcal{Q}}_q(K)$, we represent its unisolvent set of nodes with $\breve{\mathcal{N}}(K)$, i.e., the corresponding nodal values are a basis for the dual space, with cardinality $\breve{n}_\Sigma$ (see [36, Figure 1]). The corresponding shape functions and DOFs are represented with $\{\breve{\phi}^a\}_{a\in\breve{\mathcal{N}}(K)}$ and $\{\breve{\sigma}^a\}_{a\in\breve{\mathcal{N}}(K)}$, respectively. For serendipity spaces, we denote its corresponding nodal interpolator in (4) as $\breve{\pi}_K^I(v)$.

We constrain every outer DOF $a \in \mathcal{N}_h^{\text{out}}$ of a function $v_h \in \mathcal{V}_h^{\text{act}}$ as

$$v_h^a = \sigma^a(\xi_h^{\mathcal{O}(a)} \circ \breve{\pi}_{\mathcal{O}(a)}^I(v_h))) = \sum_{b\in\breve{\mathcal{N}}(\mathcal{O}(a))} \sigma^a(\xi_h^{\mathcal{O}(a)}(\breve{\phi}^b))\breve{\sigma}^b(v_h),$$

or analogously,

$$v_h(\boldsymbol{x}^a) = \sum_{b\in\breve{\mathcal{N}}(\mathcal{O}(a))} v_h(\boldsymbol{x}^b)\breve{\phi}^b(\boldsymbol{x}^a). \tag{9}$$

It leads to the new agFE space $\breve{\mathcal{V}}_h$ and its corresponding extension operator $\breve{\mathcal{E}}_h$. We note that the serendipity extension can be combined with a standard Lagrangian FE space $\mathcal{V}_h^{\text{act}}$. In fact, this is the case that will be considered in this work.

4.3. Mathematical properties. In the following, we list some FE inequalities that will be used in the next sections. We use $A \lesssim B$ to say that $A < CB$ for some positive constant C, and analogously for $\gtrsim$ and $\eqsim$. We use C to denote such a constant, which can be different in different appearances. The word *constant* in this work always denotes independence with respect to h and the cut cell intersection, i.e., it is not affected by the small cut cell problem. The constants can depend on γ and η_0. For a cut cell, h_K is defined as the one of the *whole* cell, and thus independent of the cut.

Let us consider an arbitrary FE space $\mathcal{V}_h$. The following inverse inequalities hold (see, e.g., [38]):

$$\|\boldsymbol{\nabla} u_h\|_K \lesssim h_K^{-1}\|u_h\|_K, \tag{10}$$

$$\|\partial_{\boldsymbol{n}} u_h\|_{\Gamma\cap K} \lesssim h_K^{-\frac{1}{2}}\|\boldsymbol{\nabla} u_h\|_K, \tag{11}$$

for any $K \in \mathcal{K}_h$, where $\boldsymbol{n}$ is the outward normal (in this appearance, with respect to $\Gamma_{\mathrm{D}} \cap K$), and $\partial_{\boldsymbol{n}} \doteq \boldsymbol{n} \cdot \boldsymbol{\nabla}$. The inverse inequalities (10)–(11) also hold for untrimmed aggregates $\tilde{A}$, by simply recalling them for every cell in $\tilde{A}$. Furthermore, we have the following trace inequalities (see [40]):

$$\|u\|_{\partial K} \lesssim h_K^{-\frac{1}{2}} \|u\|_K + h_K^{\frac{1}{2}} \|\boldsymbol{\nabla} u\|_K \qquad \text{for any } u \in H^1(K), \tag{12}$$

$$\|u\|_{\Gamma \cap K} \lesssim h_K^{-\frac{1}{2}} \|u\|_{\Omega \cap K} + h_K^{\frac{1}{2}} \|\boldsymbol{\nabla} u\|_{\Omega \cap K} \qquad \text{for any } u \in H^1(\Omega \cap K) \tag{13}$$

for any $K \in \mathcal{K}_h$. The last result can be proved using the ideas in [40, Lemma 3] and [41, Lemma 3.1] under the assumption that the mesh is fine enough to capture geometrical details and the curvature of Γ is bounded almost everywhere (see [40, 41] for more details). We note that for FE functions (defined in the whole cut cell K), (13) holds for both the physical and computational domain and boundary, whereas for continuous solutions it only makes sense for the physical domain. The extension operators $\mathcal{E}_h(\cdot)$ and $\breve{\mathcal{E}}_h(\cdot)$ satisfy the following stability bounds. The standard extension operator can be considered for both tet and hex meshes, whereas the serendipity extension operator only for hex meshes.

LEMMA 4.3. *Given a function $u_h \in \mathcal{V}_h^{\mathrm{in}}$, it holds that*

$$\|\mathcal{E}_h(u_h)\|_{\Omega_{\mathrm{act}}} \lesssim \|u_h\|_{\Omega_{\mathrm{in}}}, \qquad \|\breve{\mathcal{E}}_h(u_h)\|_{\Omega_{\mathrm{act}}} \lesssim \|u_h\|_{\Omega_{\mathrm{in}}},$$
$$\|\boldsymbol{\nabla}\mathcal{E}_h(u_h)\|_{\Omega_{\mathrm{act}}} \lesssim \|\boldsymbol{\nabla} u_h\|_{\Omega_{\mathrm{in}}}, \qquad \|\boldsymbol{\nabla}\breve{\mathcal{E}}_h(u_h)\|_{\Omega_{\mathrm{act}}} \lesssim \|\boldsymbol{\nabla} u_h\|_{\Omega_{\mathrm{in}}}.$$

Proof. The proof for $\mathcal{E}_h(\cdot)$ can be found in [15, Corollary 5.3] for a general agFE space, which can be either $\mathcal{V}_h^{\mathrm{in}}$ or the discontinuous FE space of its gradients. The results for $\breve{\mathcal{E}}_h(\cdot)$ can be proved analogously. ∎

The combination of the previous lemma and the inverse inequality (10) for untrimmed aggregates lead to the following global inverse inequality for functions in the agFE space:

$$\|\boldsymbol{\nabla}\mathcal{E}_h(u_h)\|_{\Omega_{\mathrm{act}}} \lesssim h^{-1} \|u_h\|_{\Omega_{\mathrm{in}}} \qquad \text{for any } u_h \in \mathcal{V}_h^{\mathrm{in}}. \tag{14}$$

Given the interior FE space $\mathcal{V}_h^{\mathrm{in}}$, we can define the standard Scott–Zhang interpolation using the definition in [42]. Let us define an *extended* Scott–Zhang interpolant as follows: (1) perform the standard interior Scott–Zhang interpolator onto $\mathcal{V}_h^{\mathrm{in}}$ through the assignment for every interior DOF $a \in \mathcal{N}_h^{\mathrm{in}}$ of an arbitrary VEF/cell[5] $\tilde{K}_a \subset \Omega_{\mathrm{in}}$ that contains the owner VEF of a, and compute the mean value of the function on $\tilde{K}_a$, represented with $\sigma_{\tilde{K}_a}^{SZ,a}(\cdot)$; (2) extend the interior function to Ω using the extension operator $\mathcal{E}_h(\cdot)$ (or $\breve{\mathcal{E}}_h(\cdot)$), leading to a function in $\mathcal{V}_h$ (or $\breve{\mathcal{V}}_h$). Thus, the extended Scott–Zhang interpolant reads

$$\pi_h^{SZ}(u)(\boldsymbol{x}) \doteq \sum_{a \in \mathcal{N}_h^{\mathrm{in}}} \sigma_{\tilde{K}_a}^{SZ,a}(u) \mathcal{E}(\phi^a(\boldsymbol{x})).$$

The serendipity-extended interpolant, represented with $\breve{\pi}_h^{SZ}(u)$, is obtained as above, but using $\breve{\mathcal{E}}_h(\cdot)$ instead.

[5] Even though this choice is arbitrary, we do not permit $\tilde{K}_a \subset \Omega_{\mathrm{in}}$ to be a vertex, since it would restrict the applicability of the interpolator to $\mathcal{C}^0(\Omega)$ functions with pointwise sense. We note that the concept of VEF/cell ownership of a DOF can be extended to nonnodal DOFs (see, e.g., [16]).

In the next theorem, we prove the approximability properties of the extended Scott–Zhang interpolant. In the statement of the theorem, we represent with $\nu(A)$ the union of the owner of the aggregate itself and the owners of all its neighbors, i.e., $\nu(A) \doteq \{\mathcal{O}(B) : A \cap B \neq \emptyset,\ B \in \mathcal{T}_h\}$. We note that $A \not\subseteq \nu(A) \subset \Omega_{\text{in}}$ in general.

THEOREM 4.4. *Let us consider an agFE space $\mathcal{V}_h$ such that $\mathcal{P}_q(A) \subset \mathcal{V}_h(A)$ for $A \in \mathcal{T}_h$, $q \in \mathbb{N}^+$. Let us consider a function $u \in W_p^m(\Omega)$, where $1 \leq p \leq \infty$, $m \leq q+1$, and $m \geq d$ for $p = 1$ or $m > \frac{d}{p}$ for $p > 1$. Given $A \in \mathcal{T}_h$ and $K \in \mathcal{K}_h$ such that $K \subseteq A$, it holds that*

$$\|u - \pi_h^{SZ}(u)\|_{W_p^s(K)} \lesssim h^{m-s}|u|_{W_p^m(\nu(A))} \tag{15}$$

for $1 \leq s \leq m$. The same results apply for the serendipity-extended agFE space $\breve{\mathcal{V}}_h$ and its corresponding interpolant $\breve{\pi}_h^{SZ}(\cdot)$.

Proof. The standard and serendipity interpolants can be analyzed analogously. The Scott–Zhang moments $\sigma_{\tilde{K}_a}^{SZ,a}(\cdot)$ are bounded in $W_p^m(\Omega)$ owing to the trace theorem, i.e., $W_p^l(\Omega) \subset L^1(\tilde{K}_a)$ for $\tilde{K}_a$ being a facet or cell (see [42]). On the other hand, $\mathcal{E}(\phi^a(\boldsymbol{x})) \subset W_p^m(K)$ for any cell $K \in \mathcal{K}_h$, since it is a combination of shape function with bounded nodal values (see (6) and Lemma 4.3). Moreover, from the definition of the extension operator, the nodal values of $\pi_h^{SZ}(\cdot)|_A$ are constrained from the DOFs of the owner interior cell of A or the DOFs of the owner cell of a neighbor of A. Thus, we readily obtain that $\|\pi_h^{SZ}(u)\|_{W_p^m(A)} \leq C\|u\|_{W_p^m(\nu(A))}$. Next, we consider an arbitrary function $\pi(u) \in W_p^m(\Omega)$ such that $\pi(u)|_K \in \mathcal{P}_q(\nu(A)) \subset \mathcal{V}_h(\nu(A))$ (note that the inclusion also holds for the serendipity extension). The fact that $\pi_h^{SZ}(\cdot)$ is a projection onto $\mathcal{V}_h$ by construction yields $\pi(u)|_A = \pi_h^{SZ}(\pi(u))|_A$. Thus, we have:

$$\begin{aligned}\|u - \pi_h^{SZ}(u)\|_{W_p^m(K)} &\leq \|u - \pi(u)\|_{W_p^m(K)} + \|\pi_h^{SZ}(\pi(u) - u)\|_{W_p^m(K)} \\ &\lesssim \|u - \pi(u)\|_{W_p^m(K)} + \|\pi(u) - u\|_{W_p^m(\nu(A))} \lesssim \|u - \pi(u)\|_{W_p^m(\nu(A))}.\end{aligned}$$

Since $\nu(A)$ is an open bounded domain with Lipschitz boundary by definition with a characteristic size bounded by γh, one can use the Deny–Lions lemma (see, e.g., [35]). As a result, using the $\pi(u)$ that minimizes the right-hand side, it holds that

$$\|u - \pi_h^{SZ}(u)\|_{W_p^m(K)} \lesssim |u|_{W_p^m(\nu(A))}.$$

The Sobolev embedding theorem and the trace theorem yield

$$\|u - \pi_h^{SZ}(u)\|_{W_p^s(K)} \leq C(A)|u|_{W_p^m(\nu(A))}. \tag{16}$$

In order to eliminate the dependency of the constant on the size of A, we use standard homogeneity (or scaling) arguments. We consider the scaling of A to a reference aggregate with unit diameter, recall (16) in the scaled domain, and use the corresponding change of variables to push back the inequality to the original aggregate (see, e.g., [38, Lemma 4.3.8] for more details). It proves the lemma. ∎

5. Approximation of the Stokes problem. In this section, we consider the FE approximation of the Stokes problem (1) using agFE spaces on unfitted meshes. We focus on inf-sup stable spaces (velocity-pressure pairs of FE spaces that satisfy a discrete version of the inf-sup condition on body-fitted meshes), which have been extended with the aggregation strategy of section 4. In this section, the velocity and pressure spaces are represented with $\boldsymbol{V}_h$ and M_h, respectively. As usual in unfitted

FE methods, the Dirichlet boundary conditions cannot be enforced strongly. Instead, we consider a Nitsche-type weak imposition of the Dirichlet data [43, 44]. It provides a consistent numerical scheme with optimal converge rates (also for high-order elements) that is commonly used in the embedded boundary community (see, e.g., [32] for its application in unfitted discretizations of the Stokes problem). Another important ingredient in unfitted FE approximations is the integration on cut cells. We refer to [14] for a detailed exposition of the particular technique used in this paper. With these ingredients, we define the Stokes operator,

$$A_h(\boldsymbol{u}_h, p_h, \boldsymbol{v}_h, q_h) \doteq a_h(\boldsymbol{u}_h, \boldsymbol{v}_h) + b_h(\boldsymbol{v}_h, p_h) - b_h(\boldsymbol{u}_h, q_h) + j_h(\boldsymbol{u}_h, p_h, \boldsymbol{v}_h, q_h), \tag{17}$$

where

$$a_h(\boldsymbol{u}_h, \boldsymbol{v}_h) \doteq (\boldsymbol{\nabla} \boldsymbol{u}_h, \boldsymbol{\nabla} \boldsymbol{v}_h)_\Omega - (\partial_{\boldsymbol{n}} \boldsymbol{u}_h, \boldsymbol{v}_h)_\Gamma - (\partial_{\boldsymbol{n}} \boldsymbol{v}_h, \boldsymbol{u}_h)_\Gamma + \tau \, (h \boldsymbol{u}_h, \boldsymbol{v}_h)_\Gamma \,, \tag{18}$$

$$b_h(\boldsymbol{v}_h, p_h) \doteq - (\boldsymbol{\nabla} \cdot \boldsymbol{v}_h, p_h)_\Omega + (\boldsymbol{n} \cdot \boldsymbol{v}_h, p_h)_\Gamma \,, \tag{19}$$

with τ a large enough positive constant, for stability purposes. The right-hand side reads

$$L_h(\boldsymbol{v}_h, q_h) \doteq (\boldsymbol{f}, \boldsymbol{v}_h)_\Omega + g_h(\boldsymbol{f}, \boldsymbol{v}_h).$$

The pressure stabilization term j_h and the corresponding potential modification of the right-hand-side g_h to keep consistency will be defined in sections 6.2 and 6.3, motivated from the numerical analysis. The discrete Stokes problem finally reads as follows: find $(\boldsymbol{u}_h,\, p_h) \in \boldsymbol{V}_h \times M_h$ such that

$$A_h(\boldsymbol{u}_h, p_h, \boldsymbol{v}_h, q_h) = L_h(\boldsymbol{v}_h, p_h) \qquad \forall \, (\boldsymbol{v}_h,\, q_h) \in \boldsymbol{V}_h \times M_h. \tag{20}$$

In the following analysis, we restrict ourselves to hexahedral meshes and discontinuous pressures. Similar ideas can be applied to inf-sup stable mixed FEs on tetrahedral meshes and continuous pressures, but we do not consider these cases for the sake of conciseness. Thus, using the notation in section 4.2, we will make use of the following global agFE spaces: the space $\mathcal{Q}_{q,h}$, for $q \geq 1$, in which the local FE space is the tensor-product Lagrangian $\mathcal{Q}_q(K)$ in all cells $K \in \mathcal{K}_h$, and the constraints are defined using the standard expression in (7); the space $\breve{\mathcal{Q}}_{q,h}$, for $q \geq 1$, in which the local FE space is the tensor-product Lagrangian $\mathcal{Q}_q(K)$ in all cells $K \in \mathcal{K}_h$, and the serendipity extension in (9) is used *only* to compute the constraints; the discontinuous space $\mathcal{P}^-_{q,h}$, for $q \geq 0$, defined in (8).

6. Numerical analysis. In this section, we perform the stability analysis of FE methods for (17). First, in section 6.1, we consider an abstract stability analysis, i.e., we prove an inf-sup condition under some assumptions over the mixed agFE space and the stabilization terms. Two different algorithms that satisfy these assumptions, and thus are stable, are proposed in sections 6.2 and 6.3. A priori error estimates for these methods are obtained in section 6.4. Finally, in section 6.5, we prove condition number bounds that are independent of the cut cell intersection with the boundary, i.e., the small cut cell problem.

The analysis of the discrete problem obviously relies on the well-posedness of the continuous problem, i.e., the inf-sup condition in (3). For the sake of conciseness in notation, we have not distinguished between the actual computational domain Ω_h and the physical domain Ω. It is important to distinguish between these two in the definition of the inf-sup constant, i.e., $\beta(\Omega)$ versus $\beta(\Omega_h)$. In general, $\beta(\Omega_h)$ can tend

to zero as $h \to 0$. The lower bound for $\beta(\cdot)$ relies on a decomposition of the domain into a finite number of strictly star-shaped domains. $\beta(\Omega_h)$ could tend to zero as $h \to 0$ unless one can prove that this number is bounded away from zero for Ω_h. Fortunately, there are constructions of the computational domain Ω_h for which one can prove that in fact $\beta(\Omega_h)$ is bounded below or, even more, converges to $\beta(\Omega)$. In particular, if Ω_h is a polygonal h-approximation of Ω in the sense of [45, Definition 4.5], it holds that $|\beta(\Omega) - \beta(\Omega_h)| \leq c(\Omega)h$. In what follows, we simply consider $\beta \doteq \inf_{h<h_0} \beta(\Omega_h)$ for h_0 a fine enough mesh size to represent the topology of the geometry at hand.

6.1. An abstract stability analysis. In this section, we analyze the well-posedness of the discretization of the Stokes problem (17) in an abstract setting, in which the FE spaces and stabilization terms are not explicitly stated. Instead, we do the analysis under some assumptions of these ingredients.

We define the following norms:

$$|||\boldsymbol{u}|||_h^2 \doteq \|\boldsymbol{\nabla u}\|_\Omega^2 + \|h^{-\frac{1}{2}}\boldsymbol{u}\|_\Gamma^2, \qquad |||\boldsymbol{u}, p|||_h^2 \doteq |||\boldsymbol{u}|||_h^2 + \|p\|_\Omega^2. \tag{21}$$

In the following lemma, we prove some stability and continuity properties of the different terms that compose the Stokes operator in (17).

LEMMA 6.1. *For a large enough positive constant τ in* (18)*, it holds for any $\boldsymbol{u}_h$, $\boldsymbol{v}_h \in \boldsymbol{V}_h$*

$$a_h(\boldsymbol{u}_h, \boldsymbol{u}_h) \geq \gamma_a |||\boldsymbol{u}_h|||_h^2, a_h(\boldsymbol{u}_h, \boldsymbol{v}_h) \leq \xi_a |||\boldsymbol{u}_h|||_h |||\boldsymbol{v}_h|||_h, b_h(\boldsymbol{v}_h, q_h) \leq \xi_b |||\boldsymbol{v}_h|||_h \|q_h\|_\Omega \tag{22}$$

for some positive constants γ_a, ξ_a, and ξ_b.

Proof. The continuity and stability of a_h can be found, e.g., in [15, Theorem 5.7]. The continuity of b_h is obtained by using in its two terms the Cauchy–Schwarz inequality and in the second one the inequalities (13) and (14) (see also [32]). ∎

Let us describe two types of common aggregate topologies. First, we define *rectangular cuboid* aggregates as the ones with such a shape (possibly after adding some inactive cells); e.g., all the aggregates in Figure 6(a) with the exception of the L-shaped aggregates on the left. Second, a *line* aggregate is such that all its cell centers lie on the same straight line. In Figure 6(a), the L-shaped and square aggregates are not line aggregates. Let us also define the set of interior aggregate facets

$$F_{AB} \doteq \partial A \cap \partial B, \quad A, B \in \mathcal{T}_h, \qquad \mathcal{F}_h \doteq \{F_{AB} : A, B \in \mathcal{T}_h\}.$$

We note that, since $A \subset \Omega$ for any aggregate $A \in \mathcal{T}_h$ by its definition in (5), F_{AB} can include a cut facet of a cut cell. Finally, we introduce below the concept of improper facets and aggregates, which will be the ones that will require some type of stabilization.

DEFINITION 6.2 (improper aggregate set of $\boldsymbol{V}_h$). *The improper aggregate set $\mathcal{T}_h^-$ is defined as the subset of aggregates in $\mathcal{T}_h$ that do not have a rectangular cuboid shape (see Figure* 6(a)*). Its complement is represented with $\mathcal{T}_h^+ \doteq \mathcal{T}_h \setminus \mathcal{T}_h^-$.*

DEFINITION 6.3 (improper facet set of $\boldsymbol{V}_h$). *The improper facet set $\mathcal{F}_h^-$ is the set of facets $F \in \mathcal{F}_h$ such that at least one the two aggregates $A_F, B_F \in \mathcal{T}_h$ that share the face is not a line aggregate (see Figure* 6(a)*). Its complement is represented with $\mathcal{F}_h^+ \doteq \mathcal{F}_h \setminus \mathcal{F}_h^-$.*

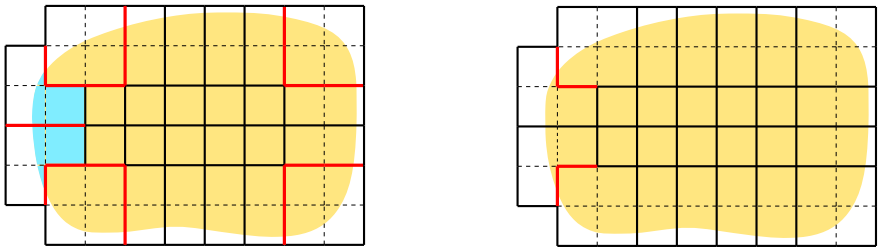

(a) Improper aggregates (in blue) in Def. 6.2 and improper facets (in red) in Def. 6.3.

(b) Reduced set of improper facets (in red) to be stabilized in Algorithm 6.13.

FIG. 6. *Illustration of improper aggregates and facets. Using Definition* 6.2*, we show in* (a) *the improper aggregates in blue. The only improper aggregates are the L-shaped ones, since the other ones have rectangular shapes. The improper facets in Definition* 6.2 *are the ones in red in* (a)*. The L-shaped aggregates and the square-shaped aggregates on the corners are not line aggregates; thus their interior boundary facets are improper. We show in* (b) *the restricted set of facets to be stabilized in the definition of Algorithm* 6.13 *in section* 6.3 *for the serendipity extension. We note that the reduced facet stabilization holds only for three dimensions and second-, third-, and fourth-order FEs with serendipity extension, but we show the idea in two dimensions for simplicity. Among all the red facets in* (a)*, only the red ones in* (b) *must be stabilized, because the other ones are between aggregates that share the same interior cell.*

In this section and section 6.2, we make the following assumption on the velocity FE space. This assumption holds, e.g., considering the velocity agFE space as the standard extension of second- or higher-order FE spaces in the interior cells.

Assumption 6.4. There exists a $q \in \mathbb{Z}^+$, $q \geq 2$, such that $\boldsymbol{\mathcal{Q}}_q(A) \subset \boldsymbol{V}_h(A)$ for any $A \in \mathcal{T}_h$.

Let us detail the roadmap that will be followed in the rest of this section in order to show the stability of (17). First, we need to prove a discrete *weak* inf-sup condition for the mixed agFE space $\boldsymbol{V}_h \times M_h$ under Assumption 6.4. In order to do that, we construct a stable *quasi*-Fortin interpolant[6] in Lemma 6.5, which is used to prove the first weak inf-sup for the space of aggregate-constant pressures in Lemma 6.6. Making use of an aggregatewise bubble function (for proper aggregates in $\mathcal{T}_h^+$ only), we can obtain extra pressure stability with additional assumptions on the mixed agFE space in Lemma 6.7. The combination of these two lemmas leads to the final weak inf-sup condition in Theorem 6.8. This result shows the *deficiency* of the weak inf-sup condition. In Assumption 6.9, we state the properties that must satisfy the pressure stabilization to correct such a deficiency. We finally prove an inf-sup condition for A_h in Theorem 6.10.

LEMMA 6.5 (quasi-Fortin interpolant). *For any $\boldsymbol{v} \in \boldsymbol{H}_{\boldsymbol{0}}^1(\Omega)$, there exists a function $\pi_h^{qF}(\boldsymbol{v}) \in \boldsymbol{V}_h$ such that*

$$\int_F \boldsymbol{v} \cdot \boldsymbol{n} = \int_F \pi_h^{qF}(\boldsymbol{v}) \cdot \boldsymbol{n} \quad \forall F \in \mathcal{F}_h^+, \quad |||\pi_h^{qF}(\boldsymbol{v})|||_h \leq \xi_{qF} \|\boldsymbol{v}\|_{1,\Omega}, \tag{23}$$

for a positive constant $\xi_{qF} > 0$.

[6] We use the name *quasi*-Fortin interpolator because it only provides the property of the standard Fortin interpolator (see, e.g., [35]) on proper facets in $\mathcal{F}_h^+$.

Proof. Facets $F \in \mathcal{F}_h^+$ are between two *line* aggregates A, $B \in \mathcal{T}_h$ by definition. This fact combined with Assumption 6.4 ensures the existence of a quadratic facet bubble such that

$$\int_F \boldsymbol{\phi}_h^F \cdot \boldsymbol{n} \gtrsim |F| > 0, \quad \|\boldsymbol{\phi}_h^F\|_\infty \lesssim 1, \quad \boldsymbol{\phi}_h^F \cdot \boldsymbol{n} = 0 \ \text{ on } \ \partial AB. \tag{24}$$

We note that the first inequality is true because A and B are line aggregates, thus there is at least one full FE facet on their interface, i.e., the one between the interior cells.

Given a function $\boldsymbol{v} \in \boldsymbol{H}_{\boldsymbol{0}}^1(\Omega)$, let us consider, e.g., the extended Scott–Zhang interpolant $\pi_h^{SZ}(\boldsymbol{v}_h)$ with the optimal approximability properties in Theorem 4.4. For agFE spaces with serendipity extensions, we would consider $\breve{\pi}_h^{SZ}(\boldsymbol{v}_h)$ instead. Using (24), at every proper facet $F \in \mathcal{F}_h^+$, we can compute $\zeta_F(\boldsymbol{v}) \in \mathbb{R}$ such that

$$\zeta_F(\boldsymbol{v}) \int_F \boldsymbol{\phi}_h^F \cdot \boldsymbol{n} = \int_F (\boldsymbol{v} - \pi_h^{SZ}(\boldsymbol{v})) \cdot \boldsymbol{n}$$

and define $\boldsymbol{\zeta}_h(\boldsymbol{v}) = \sum_{F \in \mathcal{F}_h^+} \boldsymbol{\phi}_h^F \zeta_F(\boldsymbol{v}) \in \boldsymbol{V}_h$. Thus, taking $\pi_h^{qF}(\boldsymbol{v}) \doteq \pi_h^{SZ}(\boldsymbol{v}) + \boldsymbol{\zeta}_h(\boldsymbol{v})$, one readily checks the equality in (23). Next, we prove the stability of the quasi-Fortin interpolant. We can bound $\zeta_F(\boldsymbol{v})$, since $F \in \mathcal{F}_h^+$, as follows. Let us represent with A_F, $B_F \in \mathcal{T}_h$ the two aggregates sharing F and $AB_F \doteq A_F \cup B_F$. The properties of the facet bubble in (24), the extended Scott–Zhang approximability properties in (15), the inverse inequality (13), and the Cauchy–Schwarz inequality yield

$$\begin{aligned}
|\zeta_F| &= \frac{\int_F (\boldsymbol{v} - \pi_h^{SZ}(\boldsymbol{v})) \cdot \boldsymbol{n}}{\int_F \boldsymbol{\phi}_h^F \cdot \boldsymbol{n}} \lesssim \frac{\int_F (\boldsymbol{v} - \pi_h^{SZ}(\boldsymbol{v})) \cdot \boldsymbol{n}}{|F|} \lesssim \frac{\|\boldsymbol{v} - \pi_h^{SZ}(\boldsymbol{v})\|_F}{|F|^{\frac{1}{2}}} \\
&\lesssim h^{-\frac{d-1}{2}} \|\boldsymbol{v} - \pi_h^{SZ}(\boldsymbol{v})\|_{\partial A_F} \lesssim h^{-\frac{d-1}{2}} (h^{-\frac{1}{2}} \|\boldsymbol{v} - \pi_h(\boldsymbol{v})\|_{A_F} + h^{\frac{1}{2}} |\boldsymbol{v} - \pi_h(\boldsymbol{v})|_{1,A_F}) \\
&\lesssim h^{-\frac{d-2}{2}} \|\boldsymbol{v}\|_{1,\nu(A_F)}.
\end{aligned} \tag{25}$$

Using scaling arguments, the results in (24) and (25), and the fact that for any interior cell $K \in \mathcal{K}_h^{\text{in}}$, the cardinality of the set $\{A \in \mathcal{T}_h \ : \ K \subseteq \nu(A)\}$ is bounded independently of h, we get

$$\begin{aligned}
|||\boldsymbol{\zeta}_h(\boldsymbol{v})|||_h^2 &\leq \sum_{F \in \mathcal{F}_h^+} \|\zeta_F \boldsymbol{\phi}_h^F\|_{1,AB_F}^2 \lesssim \sum_{F \in \mathcal{F}_h^+} \zeta_F^2 h^{d-2} \|\boldsymbol{\phi}_h^F\|_{L^\infty(AB_F)}^2 \\
&\lesssim \sum_{F \in \mathcal{F}_h^+} \|\boldsymbol{v}\|_{1,\nu(A_F)}^2 \lesssim \|\boldsymbol{v}\|_{1,\Omega}^2.
\end{aligned}$$

This result, combined with the stability and approximability of the Scott–Zhang projector and the triangle inequality, leads to the stability of the quasi-Fortin interpolant in (23):

$$|||\pi_h^{qF}(\boldsymbol{v})|||_h \lesssim |||\pi_h^{SZ}(\boldsymbol{v})|||_h + |||\boldsymbol{\zeta}_h(\boldsymbol{v})|||_h \lesssim \|\boldsymbol{v}\|_{1,\Omega}.$$

It proves the lemma. ∎

In what follows, we will make use of the jump operator over facets:

$$[\![p]\!](\boldsymbol{x}) = \lim_{\epsilon \to 0^+} (p(\boldsymbol{x} + \epsilon \boldsymbol{n}) - p(\boldsymbol{x} - \epsilon \boldsymbol{n})) \qquad \forall \boldsymbol{x} \in F, \ \ \forall F \in \mathcal{F}_h,$$

where $\boldsymbol{n}$ is a normal to the facet.

LEMMA 6.6. *Let us consider the mixed FE space $\boldsymbol{V}_h \times M_h$ for $M_h \doteq \mathcal{P}^-_{0,h} \cap L^2_0(\Omega)$. Then, for any $p_h \in \mathcal{P}^-_{0,h} \cap L^2_0(\Omega)$, there exists a $\boldsymbol{v}_h \in \boldsymbol{V}_h$ such that*

$$\frac{1}{\beta_0}\|p_h\|^2_\Omega \leq b_h(\boldsymbol{v}_h, p_h) + \sum_{F\in\mathcal{F}_h^-} h\|[\![p]\!]\|^2_F, \qquad |||\boldsymbol{v}_h|||_h \leq \|p_h\|_\Omega, \tag{26}$$

for a positive constant β_0.

Proof. Relying on the continuous inf-sup condition (3), for any $p_h \in \mathcal{P}^-_{0,h} \cap L^2_0(\Omega)$ there exists a $\boldsymbol{v} \in \boldsymbol{H}^1_{\boldsymbol{0}}(\Omega)$ such that

$$b_h(\boldsymbol{v}, p_h) = -(\boldsymbol{\nabla}\cdot\boldsymbol{v}, p_h)_\Omega + (\boldsymbol{v}\cdot\boldsymbol{n}, p_h)_\Gamma = -\sum_{F\in\mathcal{F}_h}(\boldsymbol{v}\cdot\boldsymbol{n}, [\![p_h]\!])_F \geq \frac{1}{\beta}\|p_h\|^2_\Omega,$$

$$\|\boldsymbol{v}\|_{1,\Omega} \lesssim \|p_h\|_\Omega, \tag{27}$$

where we have used integration by parts and added up the contributions from both cells sharing an interior facet. Using the properties of the quasi-Fortin interpolant in (23), after some algebraic manipulation, we obtain

$$\begin{aligned}
b(\pi_h^{qF}(\boldsymbol{v}), p_h) &= -\left(\boldsymbol{\nabla}\cdot\pi_h^{qF}(\boldsymbol{v}), p_h\right)_\Omega + \left(\pi_h^{qF}(\boldsymbol{v})\cdot\boldsymbol{n}, p_h\right)_\Gamma = -\sum_{F\in\mathcal{F}_h}\left(\pi_h^{qF}(\boldsymbol{v})\cdot\boldsymbol{n}, [\![p_h]\!]\right)_F \\
&= -\sum_{F\in\mathcal{F}_h^+}\left(\pi_h^{qF}(\boldsymbol{v})\cdot\boldsymbol{n}, [\![p_h]\!]\right)_F - \sum_{F\in\mathcal{F}_h^-}\left(\pi_h^{qF}(\boldsymbol{v})\cdot\boldsymbol{n}, [\![p_h]\!]\right)_F \\
&= -\sum_{F\in\mathcal{F}_h^+}(\boldsymbol{v}\cdot\boldsymbol{n}, [\![p_h]\!])_F - \sum_{F\in\mathcal{F}_h^-}\left(\pi_h^{qF}(\boldsymbol{v})\cdot\boldsymbol{n}, [\![p_h]\!]\right)_F \\
&= -\sum_{F\in\mathcal{F}_h}(\boldsymbol{v}\cdot\boldsymbol{n}, [\![p_h]\!])_F + \sum_{F\in\mathcal{F}_h^-}\left((\boldsymbol{v}-\pi_h^{qF}(\boldsymbol{v}))\cdot\boldsymbol{n}, [\![p_h]\!]\right)_F. \qquad (28)
\end{aligned}$$

We can bound the last term in (28) using the trace inequality (13), the local Scott–Zhang interpolant error estimate in Theorem 4.4 for $\boldsymbol{v} \in H^1_{\boldsymbol{0}}(\Omega)$, the second bound in (27), and Young's and Cauchy–Schwarz inequalities as follows:

$$\begin{aligned}
\sum_{F\in\mathcal{F}_h^-}\left((\boldsymbol{v}-\pi_h^{qF}(\boldsymbol{v}))\cdot\boldsymbol{n}, [\![p_h]\!]\right)_F &\leq \sum_{F\in\mathcal{F}_h^-}\|\boldsymbol{v}-\pi_h^{qF}(\boldsymbol{v})\|_F\|[\![p_h]\!]\|_F \\
&\lesssim \sum_{F\in\mathcal{F}_h^-}(h^{-\frac{1}{2}}\|\boldsymbol{v}-\pi_h^{qF}(\boldsymbol{v})\|_{A_F} \\
&\quad + h^{\frac{1}{2}}\|\boldsymbol{v}-\pi_h^{qF}(\boldsymbol{v})\|_{1,A_F})\|[\![p_h]\!]\|_F \\
&\lesssim \sum_{F\in\mathcal{F}_h^-}\|\boldsymbol{v}\|_{1,\nu(A_F)}h^{\frac{1}{2}}\|[\![p_h]\!]\|_F \\
&\lesssim \alpha\|\boldsymbol{v}\|^2_{1,\Omega} + \frac{1}{\alpha}\sum_{F\in\mathcal{F}_h^-}h\|[\![p_h]\!]\|^2_F \\
&\lesssim \alpha\|p_h\|^2_\Omega + \frac{1}{\alpha}\sum_{F\in\mathcal{F}_h^-}h\|[\![p_h]\!]\|^2_F \qquad (29)
\end{aligned}$$

for any $\alpha > 0$. Combining (27), (28), and (29) with α large enough, we readily get

$$b(\pi_h^{qF}(\boldsymbol{v}), p_h) \geq \frac{1}{\beta}\|p_h\|_\Omega^2 - C\alpha\|p_h\|_\Omega^2 - \frac{C}{\alpha}\sum_{F\in\mathcal{F}_h^-} h\|[\![p_h]\!]\|_F^2$$
$$\geq \frac{1}{\beta_0}\|p_h\|_\Omega^2 - \frac{C}{\alpha}\sum_{F\in\mathcal{F}_h^-} h\|[\![p_h]\!]\|_F^2$$

for $\beta_0 > 0$. It proves the lemma. ∎

Let us define the L^2 interpolant for extended discontinuous Lagrangian spaces as follows. Given $p_h \in \mathcal{P}_{q,h}^-$ and $0 \leq r < q$, we define $\pi_h^{-,r}(p_h) \in \mathcal{P}_{q,h}^-$ as the solution of

$$\left(\pi_h^{-,r}(p_h), q_h\right)_A = (p_h, q_h)_A \qquad \forall q_h \in \mathcal{P}_{r,h}^-.$$

LEMMA 6.7. *There exists a $\boldsymbol{\varphi}_h(p_h) \in \boldsymbol{V}_h$ that satisfies the following properties:*

(30)
$$\frac{1}{\beta_0'}\sum_{A\in\mathcal{T}_h^+}\|p_h - \pi_h^{-,0}(p_h)\|_A^2 \leq b_h(\boldsymbol{\varphi}_h(p_h), p_h), |||\boldsymbol{\varphi}_h(p_h)|||_h^2 \leq \sum_{A\in\mathcal{T}_h^+}\|p_h - \pi_h^{-,0}(p_h)\|_A^2.$$

Proof. Due to Assumption 6.4, for every proper aggregate $A \in \mathcal{T}_h^+$ (i.e., a rectangular cuboid), there is a quadratic bubble ${\boldsymbol{\phi}_h}^A \in \boldsymbol{V}_h(A)$ that vanishes on $\partial A \setminus \Gamma$ and satisfies

$$\boldsymbol{\phi}_h^A(\boldsymbol{x}) \geq 0, \int_A \boldsymbol{\phi}_h^A \gtrsim |A| > 0, \quad \|\boldsymbol{\phi}_h^A\|_\infty \lesssim 1. \tag{31}$$

For any $p_h \in M_h$, we define

$$\boldsymbol{\varphi}_h(p_h) \doteq \sum_{A\in\mathcal{T}_h^+} \phi_h^A h^2 \boldsymbol{\nabla} p_h. \tag{32}$$

Using the definition of the norms in (21), the trace inequality (13), and the inverse inequality (14), we readily obtain $|||\boldsymbol{\varphi}_h(p_h)|||_h \lesssim h^{-1}\|\boldsymbol{\varphi}_h(p_h)\|_\Omega$. Combining this result with the fact that $\|\phi_h^A\|_{\infty,A} \lesssim 1$ and (32), we prove the continuity bound in (30):

$$|||\boldsymbol{\varphi}_h(p_h)|||_h^2 \lesssim \sum_{A\in\mathcal{T}_h^+} h^2\|\boldsymbol{\nabla} p_h\|_A^2 = \sum_{A\in\mathcal{T}_h^+} h^2\|\boldsymbol{\nabla}(p_h - \pi_h^{-,0}(p_h))\|_A^2$$
$$\lesssim \sum_{A\in\mathcal{T}_h^+}\|p_h - \pi_h^{-,0}(p_h)\|_A^2.$$

Next, we note that given a proper aggregate $A \subset \mathcal{T}_h^+$ and FE function $\boldsymbol{v}_h$, using scaling arguments, the first two properties in (31), and the equivalence of norms in finite dimension, we have

$$C_-\left(\boldsymbol{v}_h, \boldsymbol{v}_h\right)_A \leq \left(\phi_h^A \boldsymbol{v}_h, \boldsymbol{v}_h\right)_A \leq C_+\left(\boldsymbol{v}_h, \boldsymbol{v}_h\right)_A \tag{33}$$

for positive constants independent of h and cut cell intersections. Thus, integrating by parts the first term in (19) and using the definition of $\boldsymbol{\varphi}_h(p_h)$ in the statement of

Lemma 6.7, the fact that aggregate bubbles vanish on interior facets on the aggregate boundaries, and the equivalence of norms in (33), we obtain

(34)
$$b_h(\boldsymbol{\varphi}_h(p_h), p_h) = \sum_{A\in\mathcal{T}_h^+} (\boldsymbol{\varphi}_h(p_h), \boldsymbol{\nabla} p_h)_A = \sum_{A\in\mathcal{T}_h^+} h^2 \left(\phi_h^A, |\boldsymbol{\nabla} p_h|^2\right)_A \gtrsim \sum_{A\in\mathcal{T}_h^+} h^2 \|\boldsymbol{\nabla} p_h\|_A^2.$$

On the other hand, since $(p_h - \pi_h^{-,0}(p_h))|_A \in M_h(A) \cap L_0^2(A)$, it holds from the Poincaré–Wirtinger inequality with a scaling argument

$$\|p_h - \pi_h^{-,0}(p_h)\|_A \lesssim h\|\boldsymbol{\nabla}(p_h - \pi_h^{-,0}(p_h))\|_A = h\|\boldsymbol{\nabla} p_h\|_A. \tag{35}$$

Combining (34) and (35), we prove the lemma. ∎

In the next theorem, we combine the inf-sup for the space of aggregate-constant pressures in Lemma 6.6 and the additional stability in Lemma 6.7 to prove the desired weak inf-sup condition.

THEOREM 6.8. *Let us assume that the mixed FE space $\boldsymbol{V}_h \times \mathcal{P}_{0,h}^- \cap L_0^2(\Omega)$ satisfies the inf-sup condition* (26) *in Lemma* 6.6. *Then, for any $p_h \in \mathcal{P}_{q-1,h}^-$, there exists a $\boldsymbol{v}_h \in \boldsymbol{V}_h$ such that*

(36)
$$\frac{1}{\beta_q}\|p_h\|_\Omega^2 \le b_h(\boldsymbol{v}_h, p_h) + \sum_{F\in\mathcal{F}_h^-} h\|[\![p_h]\!]\|_F^2 + \sum_{A\in\mathcal{T}_h^-} \|p_h + \pi_h^{-,0}(p_h)\|_A^2, \quad |||\boldsymbol{v}_h|||_h \le \|p_h\|,$$

for a positive constant β_q.

Proof. Let us decompose $b_h(\boldsymbol{v}_h, p_h)$ as follows:

$$b_h(\boldsymbol{v}_h, p_h) = b_h(\boldsymbol{v}_h, \pi_h^{-,0}(p_h)) + b_h(\boldsymbol{v}_h, p_h - \pi_h^{-,0}(p_h)). \tag{37}$$

Since $\boldsymbol{V}_h \times (\mathcal{P}_{0,h}^- \cap L_0^2(\Omega))$ is weakly inf-sup stable by the statement of the theorem, i.e., it satisfies (26), there exists a function $\boldsymbol{v}_h$ such that

(38)
$$\frac{1}{\beta_0}\|\pi_h^{-,0}(p_h)\|_\Omega^2 \le b_h(\boldsymbol{v}_h, \pi_h^{-,0}(p_h)) + \sum_{F\in\mathcal{F}_h^-} h\|[\![\pi_h^{-,0}(p_h)]\!]\|_F^2, \quad |||\boldsymbol{v}_h|||_h \le \|\pi_h^{-,0}(p_h)\|_\Omega.$$

Using the trace inequality (13), the inverse inequality (14), the stability of $\boldsymbol{v}_h$ in the weak inf-sup condition (38), and Young's and Cauchy–Schwarz inequalities, the second term in (37) can be bounded as follows:

$$\begin{aligned} b_h(\boldsymbol{v}_h, \pi_h^{-,0}(p_h) - p_h) &\lesssim \|\boldsymbol{v}_h\|_{1,\Omega}\|p_h - \pi_h^{-,0}(p_h)\|_\Omega + h^{-\frac{1}{2}}\|\boldsymbol{v}_h\|_\Gamma h^{\frac{1}{2}}\|p_h - \pi_h^{-,0}(p_h)\|_\Gamma \\ &\lesssim |||\boldsymbol{v}_h|||_h\|p_h - \pi_h^{-,0}(p_h)\|_\Omega \\ &\lesssim \alpha\|\pi_h^{-,0}(p_h)\|_\Omega^2 + \frac{1}{\alpha}\|p_h - \pi_h^{-,0}(p_h)\|_\Omega^2. \end{aligned} \tag{39}$$

Combining (37), (38), and (39) for α small enough, we get

$$\frac{1}{\beta_0^*}\|\pi_h^{-,0}(p_h)\|_\Omega^2 \le b_h(\boldsymbol{v}_h, p_h) + \sum_{F\in\mathcal{F}_h^-} h\|[\![\pi_h^{-,0}(p_h)]\!]\|_F^2 + C\|p_h - \pi_h^{-,0}(p_h)\|_\Omega^2, \tag{40}$$

where $\beta_0^* > 0$. On the other hand, we have that $\boldsymbol{\nabla} p_h \in \boldsymbol{\mathcal{P}}_{q-2,h}^-$ and $\boldsymbol{\varphi}_h(p_h) \in \boldsymbol{\mathcal{Q}}_q(A) \cap \boldsymbol{H}_0^1(A) \subset \boldsymbol{V}_h$ for any $A \in \mathcal{T}_h^+$ (see (32)). Thus, combining the first inequality in (30) from Lemma 6.7 with (40), we obtain, for an arbitrary positive constant α',

$$
\begin{aligned}
b_h(\boldsymbol{\varphi}_h(p_h) + \alpha' \boldsymbol{v}_h, p_h) &\geq \frac{1}{\beta_0'} \sum_{A \in \mathcal{T}_h^+} \|p_h - \pi_h^{-,0}(p_h)\|_A^2 + \frac{\alpha'}{\beta_0^*} \|\pi_h^{-,0}(p_h)\|_\Omega^2 \\
&\quad - \alpha' \sum_{F \in \mathcal{F}_h^-} h \|[\![\pi_h^{-,0}(p_h)]\!]\|_F^2 - \alpha' C \|p_h - \pi_h^{-,0}(p_h)\|_\Omega^2 \\
&\geq \frac{1}{\beta_0'} \sum_{A \in \mathcal{T}_h^+} \|p_h - \pi_h^{-,0}(p_h)\|_A^2 + \frac{\alpha'}{\beta_0^*} \|\pi_h^{-,0}(p_h)\|_\Omega^2 \\
&\quad - \alpha' \sum_{F \in \mathcal{F}_h^-} h \|[\![\pi_h^{-,0}(p_h)]\!]\|_F^2 \\
&\quad - \alpha' C \sum_{A \in \mathcal{T}_h^+} \|p_h - \pi_h^{-,0}(p_h)\|_A^2 - \alpha' C \sum_{A \in \mathcal{T}_h^-} \|p_h - \pi_h^{-,0}(p_h)\|_A^2 \\
&\geq \frac{1 - \alpha' C \beta_0'}{\beta_0'} \sum_{A \in \mathcal{T}_h^+} \|p_h - \pi_h^{-,0}(p_h)\|_A^2 + \frac{\alpha'}{\beta_0^*} \|\pi_h^{-,0}(p_h)\|_\Omega^2 \\
&\quad - \alpha' \sum_{F \in \mathcal{F}_h^-} h \|[\![\pi_h^{-,0}(p_h)]\!]\|_F^2 - \alpha' C \sum_{A \in \mathcal{T}_h^-} \|p_h - \pi_h^{-,0}(p_h)\|_A^2 \\
&\geq \frac{1 - \alpha' C \beta_0'}{\beta_0'} \sum_{A \in \mathcal{T}_h} \|p_h - \pi_h^{-,0}(p_h)\|_A^2 + \frac{\alpha'}{\beta_0^*} \|\pi_h^{-,0}(p_h)\|_\Omega^2 \\
&\quad - \alpha' \sum_{F \in \mathcal{F}_h^-} h \|[\![\pi_h^{-,0}(p_h)]\!]\|_F^2 \\
&\quad - \frac{1 - 2\alpha' C \beta_0'}{\beta_0'} \sum_{A \in \mathcal{T}_h^-} \|p_h - \pi_h^{-,0}(p_h)\|_A^2. \qquad (41)
\end{aligned}
$$

Next, we note that the local inverse inequality in (10) is true for untrimmed aggregates. However, since the extension operator is aggregatewise for piecewise discontinuous FE spaces, it also holds for trimmed aggregates. The trace inequality (12), the inverse inequality on trimmed aggregates, and the triangle inequality yield

$$
\begin{aligned}
\sum_{F \in \mathcal{F}_h^-} h \|[\![\pi_h^{-,0}(p_h)]\!]\|_F^2 &\leq \sum_{F \in \mathcal{F}_h^-} h \|[\![p_h - \pi_h^{-,0}(p_h)]\!]\|_F^2 + \sum_{F \in \mathcal{F}_h^-} h \|[\![p_h]\!]\|_F^2 \\
&\lesssim \sum_{A \in \mathcal{T}_h} \|p_h - \pi_h^{-,0}(p_h)\|_A^2 + \sum_{F \in \mathcal{F}_h^-} h \|[\![p_h]\!]\|_F^2. \qquad (42)
\end{aligned}
$$

Invoking (42) in (41) and picking α' small enough, we get

$$
\begin{aligned}
b_h(\boldsymbol{\varphi}_h(p_h) + \alpha' \boldsymbol{v}_h, p_h) &\gtrsim \|p_h - \pi_h^{-,0}(p_h)\|_\Omega^2 + \|\pi_h^{-,0}(p_h)\|_\Omega^2 \\
&\quad - \sum_{F \in \mathcal{F}_h^-} h \|[\![p_h]\!]\|_F^2 - \sum_{A \in \mathcal{T}_h^-} \|p_h - \pi_h^{-,0}(p_h)\|_A^2 \\
&\geq \|p_h\|_\Omega^2 - \sum_{F \in \mathcal{F}_h^-} h \|[\![p_h]\!]\|_F^2 - \sum_{A \in \mathcal{T}_h^-} \|p_h - \pi_h^{-,0}(p_h)\|_A^2.
\end{aligned}
$$

It proves the first inequality in the theorem. Furthermore, using the fact that $\|\pi_h^{-,0}(p_h)\|_\Omega \leq \|p_h\|_\Omega$, the stability in (30), and the triangle inequality, we get

$$\begin{aligned}|||\boldsymbol{\varphi}_h(p_h) + \alpha' \boldsymbol{v}_h|||_h^2 &\leq |||\boldsymbol{\varphi}_h(p_h)|||_h^2 + |||\alpha' \boldsymbol{v}_h|||_h^2 \\ &\lesssim \sum_{A \in \mathcal{T}_h^+} \|p_h - \pi_h^{-,0}(p_h)\|_A^2 + \|\alpha' \pi_h^{-,0}(p_h)\|_\Omega^2 \leq \|p_h\|_\Omega^2.\end{aligned}$$

It proves the theorem. ∎

Assumption 6.9 (pressure stabilization). For a mixed FE space $\boldsymbol{V}_h \times M_h$, we consider j_h (pressure stabilization) such that it is positive semidefinite and for any $(\boldsymbol{u}_h, p_h),\ (\boldsymbol{v}_h, q_h) \in \boldsymbol{V}_h \times M_h$ it holds that

$$\frac{1}{\gamma_j} j_h(\boldsymbol{u}_h, p_h, \boldsymbol{u}_h, p_h) \geq \sum_{A \in \mathcal{T}_h^-} \|p_h - \pi_h^{-,0}(p_h)\|_A^2 + \sum_{F \in \mathcal{F}_h^-} h \|[\![p_h]\!]\|_F^2 - \frac{\gamma_a}{2\gamma_j} |||\boldsymbol{u}_h|||_h^2, \tag{43}$$

$$j_h(\boldsymbol{u}_h, p_h, \boldsymbol{v}_h, q_h) \leq \xi_j |||\boldsymbol{u}_h, p_h|||_h |||\boldsymbol{v}_h, q_h|||_h \tag{44}$$

for some positive constants γ_j and ξ_j.

THEOREM 6.10. *Let us assume that the mixed FE space $\boldsymbol{V}_h \times M_h$ satisfies the inf-sup condition* (36) *and that the pressure stabilization j_h satisfies Assumption* 6.9. *It holds that*

$$\frac{1}{\beta_d} |||\boldsymbol{u}_h, p_h|||_h \leq \sup_{(\boldsymbol{v}_h, q_h) \in \boldsymbol{V}_h \times M_h} \frac{A_h(\boldsymbol{u}_h, p_h, \boldsymbol{v}_h, q_h)}{|||\boldsymbol{v}_h, q_h|||_h} \tag{45}$$

for a positive constant β_d.

Proof. First, we take as test function $(\boldsymbol{u}_h, p_h)$. Using the first inequality in (22), we get

$$A_h(\boldsymbol{u}_h, p_h, \boldsymbol{u}_h, p_h) = a_h(\boldsymbol{u}_h, \boldsymbol{u}_h) + j_h(\boldsymbol{u}_h, p_h, \boldsymbol{u}_h, p_h) \geq \gamma_a |||\boldsymbol{u}_h|||_h^2 + j_h(\boldsymbol{u}_h, p_h, \boldsymbol{u}_h, p_h).$$

Next, taking as test function $(\boldsymbol{v}_h, 0)$, where $\boldsymbol{v}_h$ satisfies the weak inf-sup (36) in Theorem 6.8, we get

$$\begin{aligned}A_h(\boldsymbol{u}_h, p_h, \boldsymbol{v}_h, 0) &= a_h(\boldsymbol{u}_h, \boldsymbol{v}_h) + b_h(\boldsymbol{v}_h, p_h) + j_h(\boldsymbol{u}_h, p_h, \boldsymbol{v}_h, 0) \\ &\geq \frac{1}{\beta_q} \|p_h\|_\Omega^2 - \sum_{F \in \mathcal{F}_h^-} h \|[\![p_h]\!]\|_F^2 - \sum_{A \in \mathcal{T}_h^-} \|p_h - \pi_h^{-,0} p_h\|_A^2 \\ &\quad + a_h(\boldsymbol{u}_h, \boldsymbol{v}_h) + j_h(\boldsymbol{u}_h, p_h, \boldsymbol{v}_h, 0).\end{aligned} \tag{46}$$

On one side, the second inequality in (22) together with Young's and Cauchy–Schwarz inequalities yields

$$a_h(\boldsymbol{u}_h, \boldsymbol{v}_h) \leq \frac{\xi_a^2}{4\alpha} |||\boldsymbol{u}_h|||_h^2 + \alpha |||\boldsymbol{v}_h|||_h^2 \leq \frac{\xi_a^2}{4\alpha} |||\boldsymbol{u}_h|||_h^2 + \alpha \|p_h\|_\Omega^2$$

for an arbitrary constant α. On the other side, using the fact that the pressure stabilization is positive semidefinite, Cauchy–Schwarz and Young's inequalities, the continuity in (44), and the stability for $\boldsymbol{v}_h$ in (36), we get

$$
\begin{aligned}
j_h(\boldsymbol{u}_h,p_h,\boldsymbol{v}_h,0) &\geq -\frac{1}{4\alpha}j_h(\boldsymbol{u}_h,p_h,\boldsymbol{u}_h,p_h)-\alpha j_h(\boldsymbol{v}_h,0,\boldsymbol{v}_h,0)\\
&\geq -\frac{1}{4\alpha}j_h(\boldsymbol{u}_h,p_h,\boldsymbol{u}_h,p_h)-\alpha\xi_j|||\boldsymbol{v}_h|||_h^2\\
&\geq -\frac{1}{4\alpha}j_h(\boldsymbol{u}_h,p_h,\boldsymbol{u}_h,p_h)-\alpha\xi_j\|p_h\|_\Omega^2. \qquad (47)
\end{aligned}
$$

As a result, combining (46)–(47), and taking α small enough, we obtain

$$
\begin{aligned}
A_h(\boldsymbol{u}_h,p_h,\boldsymbol{v}_h,0) \gtrsim \|p_h\|_\Omega^2 &- \sum_{F\in\mathcal{F}_h^-} h\|[\![p_h]\!]\|_F^2 - \sum_{A\in\mathcal{T}_h^-}\|p_h-\pi_h^{-,0}(p_h)\|_A^2\\
&- j_h(\boldsymbol{u}_h,p_h,\boldsymbol{u}_h,p_h)-|||\boldsymbol{u}_h|||_h^2. \qquad (48)
\end{aligned}
$$

By taking $(\boldsymbol{u}_h+\alpha'\boldsymbol{v}_h,p_h)$ as a test function with α' small enough, using (47), (48), and the assumption over the pressure stability in (43), we finally get

$$
\begin{aligned}
A_h(\boldsymbol{u}_h,p_h,\boldsymbol{u}_h+\alpha'\boldsymbol{v}_h,p_h) &\gtrsim |||\boldsymbol{u}_h|||_h^2+\alpha' C\|p_h\|_\Omega^2+j_h(\boldsymbol{u}_h,p_h,\boldsymbol{u}_h,p_h)\\
&\quad -\alpha' C\sum_{F\in\mathcal{F}_h^-} h\|[\![p_h]\!]\|_F^2-\alpha' C\sum_{A\in\mathcal{T}_h^-}\|p_h-\pi_h^{-,0}(p_h)\|_A^2\\
&\gtrsim |||\boldsymbol{u}_h|||_h^2+\|p_h\|_\Omega^2+j_h(\boldsymbol{u}_h,p_h,\boldsymbol{u}_h,p_h).
\end{aligned}
$$

On the other hand, the stability for $\boldsymbol{v}_h$ in (36) and the triangle inequality yield

$$
|||\boldsymbol{u}_h+\alpha'\boldsymbol{v}_h,p_h|||_h \lesssim |||\boldsymbol{u}_h,p_h|||_h+|||\alpha'\boldsymbol{v}_h|||_h \lesssim |||\boldsymbol{u}_h,p_h|||_h+\|\alpha' p_h\|_\Omega \lesssim |||\boldsymbol{u}_h,p_h|||_h.
$$

It proves the theorem. ∎

6.2. Mixed agFEM and pressure stabilization. We propose below an algorithm that satisfies Assumption 6.9 and thus the stability results in Theorem 6.10.

ALGORITHM 6.11. *We consider a hex mesh, the velocity space* $\boldsymbol{V}_h \doteq \boldsymbol{\mathcal{Q}}_{q,h}$, *and the pressure space* $M_h \doteq \mathcal{P}^-_{q-1,h}$ *for an integer* $q\geq 2$. *The pressure stabilization term is taken as*

$$
\begin{aligned}
j_h(\boldsymbol{u}_h,p_h,\boldsymbol{v}_h,q_h) &\doteq \sum_{F\in\mathcal{F}_h^-}\tau_{j1}h\left([\![p_h]\!],[\![q_h]\!]\right)_F+\sum_{A\in\mathcal{T}_h^-}\tau_{j2}h^2\left(-\Delta\boldsymbol{u}_h+\boldsymbol{\nabla}p_h,-\Delta\boldsymbol{v}_h+\boldsymbol{\nabla}q_h\right)_A,\\
g_h(\boldsymbol{f},\boldsymbol{v}_h) &\doteq \sum_{A\in\mathcal{T}_h^-}h^2\left(\boldsymbol{f},-\Delta\boldsymbol{v}_h+\boldsymbol{\nabla}q_h\right)_A \qquad (49)
\end{aligned}
$$

for positive algorithmic constants τ_{j1} *and* τ_{j2}.

The agFE space thus relies on the popular FE space $\boldsymbol{\mathcal{Q}}_{q,h}\times\mathcal{P}^-_{q-1,h}$ for the interior cells. The velocity field is extended to cut cells by the standard extension operator in section 4.2.3, and the discontinuous pressure field is extended by the standard (discontinuous) one. This choice has been motivated by the proof of the abstract discrete inf-sup condition.

THEOREM 6.12. *The method proposed in Algorithm* 6.11 *has a pressure stabilization term that satisfies Assumption* 6.9 *and thus it satisfies Theorem* 6.10. *As a result, the discrete problem* (20) *is well-posed for* $\boldsymbol{f}\in\boldsymbol{L}^2(\Omega)$.

Proof. As required in Assumption 6.9, the pressure stabilization is positive semidefinite. In order to prove that (43) holds, we use the following inequality. Given three functions v, p in a Hilbert space X and u in a Banach space Y, defining $\gamma^{\frac{1}{2}} \doteq \frac{\|u\|_Y}{\|v\|_X}$, we have, using Young's inequality for an arbitrary constant $\alpha > 1$,

$$\begin{aligned} 2\|p-v\|_X^2 &= \|p-v\|_X^2 + \|p\|_X^2 + \|v\|_X^2 - 2(p,v)_X \\ &\geq \|p-v\|_X^2 + \left(1-\frac{1}{\alpha}\right)\|p\|_X^2 - (\alpha-1)\|v\|_X^2 \\ &= \|p+v\|_X^2 + \left(1-\frac{1}{\alpha}\right)\|p\|_X^2 - \frac{\alpha-1}{\gamma}\|u\|_Y^2. \end{aligned}$$

Taking $\alpha = 1+\gamma > 1$, we obtain

$$2\|p+v\|_X^2 \geq \|p+v\|_X^2 + \frac{1}{1+\frac{1}{\gamma}}\|p\|_X^2 - \|u\|_Y^2.$$

Let us consider $X = L^2(A)$, $v = h\Delta \boldsymbol{u}_h$, $p = h\boldsymbol{\nabla} p_h$, $Y = \boldsymbol{H}^1(A)$, and $u = \omega^{\frac{1}{2}}\boldsymbol{u}_h$, for $A \in \mathcal{T}_h^-$ and an arbitrary positive constant ω. Using the inverse inequality (10), we have that $h\|\Delta \boldsymbol{u}_h\|_A \leq C\|\boldsymbol{u}_h\|_{1,\tilde{A}}$, thus $\gamma \geq C^{-2}\omega$. The previous bound leads to

$$\sum_{A\in\mathcal{T}_h^-} h^2\| -\Delta \boldsymbol{u}_h + \boldsymbol{\nabla} p_h\|_A^2 \geq C \sum_{A\in\mathcal{T}_h^-} h^2\|\boldsymbol{\nabla} p_h\|_\Omega^2 - \sum_{A\in\mathcal{T}_h^-} \omega\|\boldsymbol{u}_h\|_{1,\tilde{A}}^2. \tag{50}$$

The Poincaré–Wirtinger inequality with a scaling argument yields

$$\|p_h - \pi_h^{-,0}(p_h)\|_A \lesssim h\|\boldsymbol{\nabla}(p_h - \pi_h^{-,0}(p_h)\|_\Omega = h\|\boldsymbol{\nabla} p_h\|_\Omega. \tag{51}$$

Combining (50) and (51), using Lemma 4.3, and adjusting ω accordingly, we find

$$j_h(\boldsymbol{u}_h, p_h, \boldsymbol{u}_h, p_h) \geq \gamma_j \sum_{A\in\mathcal{T}_h^-} \|p_h - \pi_h^{-,0}(p_h)\|_A^2 + \gamma_j \sum_{F\in\mathcal{F}_h^-} h\|[\![p_h]\!]\|_F^2 - \frac{\gamma_a}{2\gamma_j}\|\boldsymbol{u}_h\|_{1,\Omega}^2$$

for a positive constant γ_j. Thus, the stabilization term satisfies Assumption 6.9. Its continuity in (44) is obtained from the trace inequalities (12)–(13) and the inverse inequality (14). This result, together with (45), proves the well-posedness of the discrete operator. Furthermore, for $\boldsymbol{f} \in L_0^2(\Omega)$, we can easily prove that $g_h(\boldsymbol{f}, \boldsymbol{v}_h) \leq \xi_g\|\boldsymbol{f}\|_\Omega |||\boldsymbol{v}_h|||_h$. ∎

6.3. Mixed agFEM with serendipity extension. In this section, we propose another mixed agFEM, which makes use of the serendipity extension in section 4.2.3. It relies again on $\boldsymbol{\mathcal{Q}}_{q,h} \times \mathcal{P}_{q-1,h}^-$ for the interior cells. The velocity field is extended to cut cells by the serendipity extension operator and the discontinuous pressure field is extended by the standard (discontinuous) one. This choice has also been motivated by the proof of the abstract discrete inf-sup condition. The method reads as follows.

ALGORITHM 6.13. *We consider a hex mesh, the velocity space* $\boldsymbol{V}_h \doteq \breve{\boldsymbol{\mathcal{Q}}}_{q,h}$, *and the pressure space* $M_h \doteq \mathcal{P}_{q-1,h}^-$ *for an integer* $2 \leq q \leq 2d-2$. *The pressure stabilization term is taken as*

$$j_h(p_h, q_h) \doteq \sum_{F\in\mathcal{F}_h^-} \tau_{j1} h \left([\![p_h]\!], [\![q_h]\!]\right)_F \tag{52}$$

for a positive algorithmic constant τ_{j1}, whereas $g_h(\boldsymbol{f}, \boldsymbol{v}_h) \doteq 0$. In three dimensions, if $q \leq 2d-3$, the improper facet set $\mathcal{F}_h^-$ can be reduced further, by considering only those facets that also satisfy that their corresponding owner interior cells $\mathcal{O}(A_F)$ and $\mathcal{O}(B_F)$ do not share a FE facet, i.e., $|K_{A_F} \cap K_{B_F}| = \emptyset$ in $d-1$ sense (see Figure 6(b)*).*

We note that Assumption 6.4 does not hold in this case but stability is proved using a different strategy. The analysis is almost identical to the one in section 6.1. We only comment on the two points in which it differs.

THEOREM 6.14. *The method proposed in Algorithm* 6.13 *has a pressure stabilization term that satisfies Assumption* 6.9 *and thus it satisfies Theorem* 6.10*. As a result, the discrete problem* (20) *is well-posed for $\boldsymbol{f} \in \boldsymbol{H}^{-1}(\Omega)$.*

Proof. First, we note that for the serendipity FE up to order $2d-2$, a unisolvent set of DOFs are nodal values on the cell boundary only and thus zero for bubble functions (see [36] for more details). Thus, the serendipity extension of the quadratic bubble function of the owner cell of the aggregate is zero in $\Omega \setminus \Omega_{\text{in}}$ for $q \leq 2d-2$. Therefore, one can define aggregate bubbles that satisfy (31) for *all* the aggregates; thus all the lemmas/theorems still apply without the need of cell interior stabilization or Assumption 6.4.

In three dimensions, since serendipity FEs up to order $2d-3$ do not include the DOFs corresponding to the quadratic facet bubbles, the facet bubbles of the owner interior cells of an aggregate are extended by zero. Thus, if the roots of two neighboring aggregates are also neighbors, there exists a facet bubble that satisfies (24). As a result, the subset $\mathcal{F}_h^-$ can be restricted as stated in the definition of the algorithm, whereas the previous lemmas/theorems still hold (see Figure 6(b)). On the other hand,

$$j_h(\boldsymbol{u}_h, p_h, \boldsymbol{u}_h, p_h) = \sum_{F \in \mathcal{F}_h^-} \tau_{j1} h \|[\![p_h]\!]\|_F^2.$$

We can readily check that the stabilization term satisfies (43). The continuity result in (44) is readily obtained from the trace inequalities (12)–(13). As a result, the stabilization term satisfies Assumption 6.9. This result, together with (45), proves the theorem. ∎

6.4. A priori error estimates. At this point, we have already checked that Algorithms 6.11 and 6.13 are well-posed. Next, we want to prove a priori error estimates for these algorithms. The proof of these results is fairly straightforward, since the pressure stabilization terms are consistent for pressure fields in $H^1(\Omega)$. As usual, Galerkin orthogonality, the stability in Theorems 6.12 and 6.14, and the approximability properties in Theorem 4.4 lead to the desired results.

Let us note that the jump stabilization in (52) (also in (49)) can be modified by integrating not only on (potentially) cut facets $F \in \mathcal{F}_h$ but in the corresponding whole facets. Such modification does provide more stabilization and does not affect the consistency of the method in the error analysis of Theorem 6.15 below.

THEOREM 6.15. *Let us consider the discrete solution $(\boldsymbol{u}_h, p_h) \in \boldsymbol{V}_h \times M_h$ in Algorithms* 6.11 *and* 6.13 *(for a given order $q \geq 1$). If the solution $(\boldsymbol{u}, p)$ of the Stokes problem* (2) *belongs to $\boldsymbol{H}^{\alpha+1}(\Omega) \times H^{\alpha}(\Omega)$ for $\alpha \geq 1$, then the following* a priori *error estimate holds for $k \doteq \min(q, \alpha)$:*

$$|||\boldsymbol{u} - \boldsymbol{u}_h, p - p_h|||_h \lesssim h^k \|\boldsymbol{u}\|_{H^{k+1}(\Omega)} + h^k \|p\|_{H^k(\Omega)}.$$

Proof. First, let us note that the bilinear form A_h in Algorithms 6.11 and 6.13 is consistent. Since $p \in H^1(\Omega)$, the pressure jump stabilization vanishes. It is obvious to check that the interior residual-based stabilization vanishes too. Let us consider the extended Scott–Zhang projector for every component of the velocity $\pi_h^{SZ}(\boldsymbol{u})$ and for the pressure $\pi_h^{SZ}(p)$. The Galerkin orthogonality and the continuity of A_h (which is a direct consequence of the continuity results in (22)–(44)) yield

$$\begin{aligned} A_h(\boldsymbol{u}_h - \pi_h^{SZ}(\boldsymbol{u}), p_h - \pi_h^{SZ}(p), \boldsymbol{v}_h, q_h) &= A_h(\boldsymbol{u} - \pi_h^{SZ}(\boldsymbol{u}), p - \pi_h^{SZ}(p), \boldsymbol{v}_h, q_h) \\ &\leq \xi_A |||\boldsymbol{u} - \pi_h^{SZ}(\boldsymbol{u}), p - \pi_h^{SZ} p|||_h |||\boldsymbol{v}_h, q_h|||_h. \end{aligned}$$

Taking as test function the $(\boldsymbol{v}_h, q_h)$ for which the global inf-sup condition in Theorem 6.10 is satisfied and the previous inequality, we readily get

$$\begin{aligned} |||\boldsymbol{u}_h - \pi_h^{SZ}(\boldsymbol{u}), p_h - \pi_h^{SZ}(p)|||_h &\leq \beta_d \frac{A_h(\boldsymbol{u}_h - \pi_h^{SZ}(\boldsymbol{u}), p_h - \pi_h^{SZ}(p), \boldsymbol{v}_h, q_h)}{|||\boldsymbol{v}_h, q_h|||_h} \\ &\leq \beta_d \xi_A |||\boldsymbol{u} - \pi_h^{SZ}(\boldsymbol{u}), p - \pi_h^{SZ}(p)|||_h. \end{aligned}$$

Finally, the approximability properties of the extended Scott–Zhang projector in Theorem 4.4 and the trace inequality (13) yield

$$\begin{aligned} |||\boldsymbol{u} - \pi_h^{SZ}(\boldsymbol{u}), p - \pi_h^{SZ} p|||_h^2 &= \|\boldsymbol{\nabla}(\boldsymbol{u} - \pi_h^{SZ}(\boldsymbol{u}))\|_\Omega^2 + \|h^{-\frac{1}{2}}(\boldsymbol{u} - \pi_h^{SZ}(\boldsymbol{u}))\|_\Gamma^2 + \|p - \pi_h^{SZ} p\|_\Omega^2 \\ &\lesssim h^{2k} \|\boldsymbol{u}\|_{H^{k+1}(\Omega)}^2 + h^{2k} \|p\|_{H^k(\Omega)}^2. \end{aligned}$$

It proves the theorem. ∎

6.5. Condition number bounds. It is well-known that extended FE spaces without aggregation lead to arbitrary ill-conditioned systems, due to the small cut cell problem, i.e., when the ratio η_K tends to zero (see [12] for details). Thus, arbitrarily high condition numbers are expected in practice since the position of the interface cannot be controlled and the value η_K can be arbitrarily close to zero. It has motivated the agFEM in [15]. We prove in the following theorem that the agFEM proposed herein for the Stokes problem leads to the same condition number bounds as for body-fitted methods, i.e., they do not depend on the cut cell intersection. We represent with $|\cdot|_{\ell^2}$ the Euclidean norm of vectors and matrices.

THEOREM 6.16. *The condition number of the matrices that arise from Algorithms* 6.11 *and* 6.13*, i.e.,* $\kappa(A_h) \doteq |A_h|_{\ell^2} |A_h^{-1}|_{\ell^2}$*, satisfies* $\kappa(A_h) \leq C_\kappa h^{-2}$ *for a positive constant* C_κ*.*

Proof. First, we note that $\boldsymbol{u}_h \in \boldsymbol{V}_h$ can be stated in terms of a global basis of FE shape functions as $\sum_{a=1}^{N_u} U_a \boldsymbol{\phi}_u^a$. We define the Cartesian norm for the vector of DOF values of $\boldsymbol{u}_h$ as $|\boldsymbol{u}_h|_{\ell^2}$. We proceed analogously for the pressure, e.g., $p_h = \sum_{a=1}^{N_p} P_a \phi_p^a \in M_h$; we note that the pressure space has dimension $N_p - 1$ due to the zero mean restriction, i.e., $M_h \subset L_0^2(\Omega)$. Let us represent velocity-pressure functions in $\boldsymbol{V}_h \times M_h$ with bold capital Greek letters. Given $\boldsymbol{\Phi}_h \doteq (\boldsymbol{u}_h, p_h)$, we define $|\boldsymbol{\Phi}_h|_{\ell^2}^2 \doteq |\boldsymbol{u}_h|_{\ell^2}^2 + |p_h|_{\ell^2}^2$. For any velocity component and pressure, we have from the fact that the eigenvalues of the local mass matrix in every interior cell are bounded (see, e.g., [46]) that $C_m^- h^d |\boldsymbol{u}_h|_{\ell^2}^2 \leq \|u_h\|_{\Omega_{\text{in}}}^2 \leq C_m^+ h^d |\boldsymbol{u}_h|_{\ell^2}^2$. This result, combined with the stability of the extension operator in Lemma 4.3, yields

$$C_M^- h^d |\boldsymbol{u}_h|_{\ell^2}^2 \leq \|\boldsymbol{u}_h\|_\Omega^2 \leq C_M^+ h^d |\boldsymbol{u}_h|_{\ell^2}^2. \tag{53}$$

We can proceed analogously for the pressure space. Now, we can bound the following velocity norm using the inverse inequality (14), the trace inequality (12), and the norm relation in (53), as follows:

$$|||\boldsymbol{u}_h|||_h^2 = \|\boldsymbol{\nabla}\boldsymbol{u}_h\|_\Omega^2 + \|h^{-\frac{1}{2}}\boldsymbol{u}_h\|_\Gamma^2 \lesssim h^{-2}\|\boldsymbol{u}_h\|_\Omega^2 \lesssim h^{d-2}|\boldsymbol{u}_h|_{\ell^2}^2.$$

Thus, we have $|||\boldsymbol{\Phi}_h|||_h^2 \lesssim h^{d-2}|\boldsymbol{\Phi}_h|_{\ell^2}^2$ for any $\boldsymbol{\Phi}_h \in \boldsymbol{V}_h \times M_h$. The Friedrichs inequality and (53) yield $|\boldsymbol{u}_h|_{\ell^2}^2 \leq C(\Omega)h^{-d}\|\boldsymbol{u}_h\|_\Omega^2 \lesssim C(\Omega)h^{-d}|||\boldsymbol{u}_h|||_h^2$. As a result,

$$C(\Omega)^{-1}h^d|\boldsymbol{u}_h|_{\ell^2}^2 \lesssim |||\boldsymbol{u}_h|||_h^2 \lesssim h^{d-2}|\boldsymbol{u}_h|_{\ell^2}^2. \tag{54}$$

We can bound the norm of A_h by using its continuity (from the continuity results in (22) and (44)) and the norm equivalence in (54) for the velocity and the version in (53) for the pressure as follows:

$$|A_h|_{\ell^2} = \max_{\boldsymbol{\Phi}_h \in \boldsymbol{V}_h \times M_h} \max_{\boldsymbol{\Psi}_h \in \boldsymbol{V}_h \times M_h} \frac{A_h(\boldsymbol{\Phi}_h, \boldsymbol{\Psi}_h)}{|\boldsymbol{\Phi}_h|_{\ell^2}|\boldsymbol{\Psi}_h|_{\ell^2}} \leq \xi_A \frac{|||\boldsymbol{\Phi}_h|||_h |||\boldsymbol{\Psi}_h|||_h}{|\boldsymbol{\Phi}_h|_{\ell^2}|\boldsymbol{\Psi}_h|_{\ell^2}} \lesssim h^{d-2}. \tag{55}$$

Making abuse of notation, we use $A_h\boldsymbol{\Phi}_h \doteq A_h(\boldsymbol{\Phi}_h, \cdot)$. Next, we provide a lower bound for the norm of the operator $A_h\boldsymbol{\Phi}_h$ for some $\boldsymbol{\Phi}_h \in \boldsymbol{V}_h \times M_h$. Using the inf-sup condition in Theorem 6.10 and the norm equivalence in (54), we obtain

$$\begin{aligned} |A_h\boldsymbol{\Phi}_h|_{\ell^2} &= \max_{\boldsymbol{\Psi}_h \in \boldsymbol{V}_h \times M_h} \frac{A_h(\boldsymbol{\Phi}_h, \boldsymbol{\Psi}_h)}{|\boldsymbol{\Psi}_h|_{\ell^2}} \\ &= \max_{\boldsymbol{\Psi}_h \in \boldsymbol{V}_h \times M_h} \frac{A_h(\boldsymbol{\Phi}_h, \boldsymbol{\Psi}_h)}{|||\boldsymbol{\Psi}_h|||_h} \frac{|||\boldsymbol{\Psi}_h|||_h}{|\boldsymbol{\Psi}_h|_{\ell^2}} \geq \beta_d |||\boldsymbol{\Phi}_h|||_h \min_{\boldsymbol{\Psi}_h \in \boldsymbol{V}_h \times M_h} \frac{|||\boldsymbol{\Psi}_h|||_h}{|\boldsymbol{\Psi}_h|_{\ell^2}}. \end{aligned} \tag{56}$$

Combining (56) and the lower bound in (54), we get $|A_h\boldsymbol{\Phi}_h|_{\ell^2} \gtrsim h^d|\boldsymbol{\Phi}_h|_{\ell^2}$. Taking $\boldsymbol{\Phi}_h = A_h^{-1}\boldsymbol{\Psi}_h$, we readily obtain $|\boldsymbol{\Psi}_h|_{\ell^2} \gtrsim h^d|A_h^{-1}\boldsymbol{\Psi}_h|_{\ell^2}$. Thus, $|A_h^{-1}|_{\ell^2} \lesssim h^{-d}$, which, together with (55), proves the theorem. ∎

7. Numerical experiments. The main purpose of this section is to evaluate the performance of the agFE spaces in several different scenarios. We start with a convergence test (cf. section 7.2), where we numerically validate the a priori error estimates of section 6.4 and the condition number bounds of section 6.5. Next, we consider a moving domain test (cf. section 7.3) in order to check the robustness of the methods with respect to small cuts. Finally, we provide the numerical solution of two realistic problems (cf. section 7.4) in order to illustrate the ability of the agFEM to deal with complex geometrical data. The performance of the linear solver step is not analyzed herein. The implementation of optimal and scalable solvers for the Stokes problem and its application to agFEM will be considered in future work.

7.1. Setup. In all cases, we solve the Stokes problem (1) using Galerkin approximations with conforming Lagrangian FE spaces as indicated in section 5. We consider both agFE spaces and conventional ones in order to evaluate the benefits of using cell aggregation. For the conventional (unaggregated) case, we use, in all cells $K \in \mathcal{K}_h$, $\mathcal{Q}_{2,h}$ and $\mathcal{P}_{1,h}^-$ spaces for the approximation of velocities and pressures, respectively (e.g., in three dimensions, hexahedral elements with continuous piecewise triquadratic shape functions for the velocity, and discontinuous piecewise linear shape functions for the pressure). For the aggregated case, we consider Algorithm 6.13 with $q = 2$, i.e., the space $\breve{\mathcal{Q}}_{2,h}$ for every velocity component (the aggregated version of $\mathcal{Q}_{2,h}$ using the serendipity extension in section 4.2.3) and the aggregated counterpart of $\mathcal{P}_{1,h}^-$ for

the pressure. In order to fulfill inf-sup stability, we use the facet-based stabilization given in (52) for the aggregated spaces with $\tau_{j1} = 0.01$ (the value that minimized the error for a simple test and a set of possible constants). The results for the usual (unaggregated) spaces are labeled as *standard* throughout the numerical examples, whereas results using cell aggregation are labeled as *aggregated*.

The algorithms proposed in this work have been implemented using the tools provided by the object-oriented HPC code `FEMPAR` [16]. The underlying systems of linear equations are solved by means of a robust sparse direct solver from the MKL PARDISO package [47] specially designed for symmetric indefinite matrices (to which `FEMPAR` provides appropriate interfaces). The condition number estimates provided below are computed outside `FEMPAR` using the MATLAB function `condest`. Numerical integration is based on local body-fitted triangulations of cut cells into triangles (in two dimensions) or tetrahedra (in three dimensions), where standard quadrature rules can be applied. The local triangulation of a cut cell is obtained by `FEMPAR` from its nodal coordinates and the intersection points of cell edges with the unfitted boundary via the Delaunay method available in the `QHULL` library [48, 49]. Note that these submeshes are used only for integration purposes and are completely independent from one cut cell to another (see [14] for details).

7.2. Convergence test. We consider the Stokes problems defined in the 2D and 3D domains shown in Figure 7. The 2D domain (cf. Figure 7(a)) is a circular cavity defined as the set difference of the unit square $[0,1]^2$ and the circle of radius $R = 0.3$ and center $C = (0.5, 0.5)$. The 3D domain is a complex-shaped cavity defined as the set difference of the unit cube $[0,1]^3$ and a 3D body whose shape reminds the one of a popcorn flake (cf. Figures 7(b) and 7(c)). This "popcorn-flake" geometry is often used in the literature to study the performance of unfitted FE methods (see, e.g., [8]). The popcorn flake geometry considered here is obtained by taking the one defined in [8], scaling it by a factor of 0.5 and translating it a value of 0.5 in each direction such that the body fits in the unit cube $[0,1]^3$. We consider Dirichlet boundary conditions on the interior walls of the cavities, whereas Neumann conditions are imposed on the facets of the unit square and unit cube (see Figure 7). Dirichlet boundary conditions are imposed using Nitsche's method as discussed in section 5.

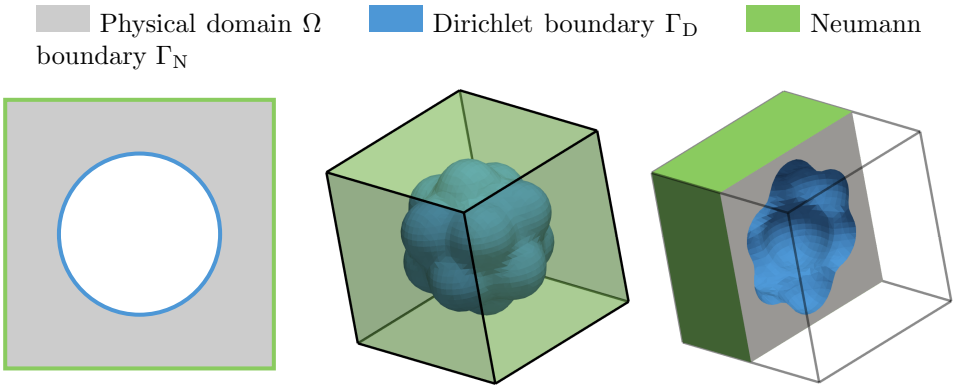

(a) 2D case. (b) 3D case (outer view). (c) 3D case (internal view).

FIG. 7. *Convergence test: View of the problem geometries.*

We use the method of manufactured solutions in order to have a problem with known exact solution, which is used here to compute discretization errors. The (manufactured) exact solution we have considered is

$$\boldsymbol{u} \doteq \frac{\boldsymbol{u}^*}{|\boldsymbol{u}^*|}, \qquad p \doteq x^3 y^3, \tag{57}$$

where

$$\begin{aligned} &\boldsymbol{u}^* = (-y + 0.5,\ x + 0.3)^t, \quad (x, y) \in \Omega \subset \mathbb{R}^2 \quad \text{in two dimensions,} \\ &\boldsymbol{u}^* = (y - 0.5,\ -x - z - 0.3,\ y - 0.5)^t, \quad (x, y, z) \in \Omega \subset \mathbb{R}^3 \quad \text{in three dimensions.} \end{aligned}$$

This solution corresponds to a (divergence-free) velocity field of magnitude 1 that spins around the point $(x, y) = (-0.3, 0.5)$ for the 2D case and around the line $(x, y, z) = (-z - 0.3, 0.5, z)$, $z \in \mathbb{R}$, in three dimensions (see Figure 8). The particular values of the boundary conditions (both Dirichlet and Neumann) and external loads are defined such that (57) is the exact solution of the Stokes problem (1).

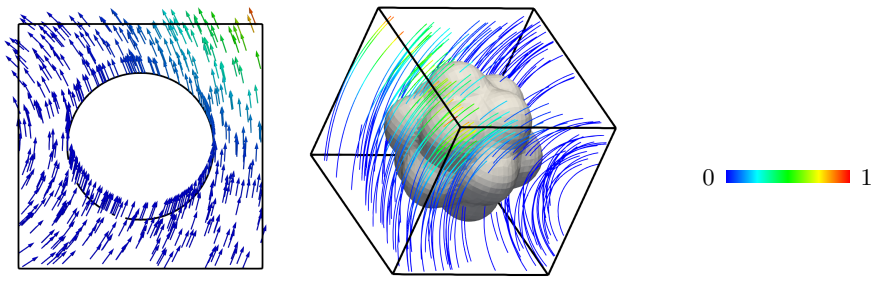

(a) 2D case. (b) 3D case.

FIG. 8. *Convergence test: View of the manufactured solution (vectors/streamlines colored by pressure field).*

The numerical approximation is done using a family of uniform Cartesian meshes obtained by dividing each direction of the unit square and cube into 2^m parts, with $m = 3, 4, \ldots, 9$ in two dimensions and $m = 3, 4, 5$ in three dimensions. The obtained results are displayed in Figures 9, 10, and 11.

Figure 9 shows the scaling of the condition number of the underlying linear systems as the mesh is refined. For the agFE spaces, the condition number scales as expected in conventional FE methods for body-fitted meshes (i.e., the condition number is proportional to h^{-2}), which confirms the theoretical condition number bound derived in section 6.5. The same behavior is observed in 2D and 3D cases. The lines for the 3D case in Figure 9(b) have only two points, since we were able to estimate the condition number only for two of the 3D meshes due to the large amount of memory demanded by the `condest` function of MATLAB. The benefit of using cell aggregation is clearly illustrated in Figure 9. The standard FE spaces without cell aggregation lead to condition numbers that do not scale proportional to h^{-2}. Theoretically, the condition number can be arbitrarily large without cell aggregation depending on how cells are cut, which leads in practice to an erratic scaling of the condition number that reaches large values, as shown by the red lines in Figure 9.

On the other hand, Figures 10 and 11 report the convergence of the H^1 seminorm and L^2 norm of the discretization error for the velocity field, and the L^2 norm

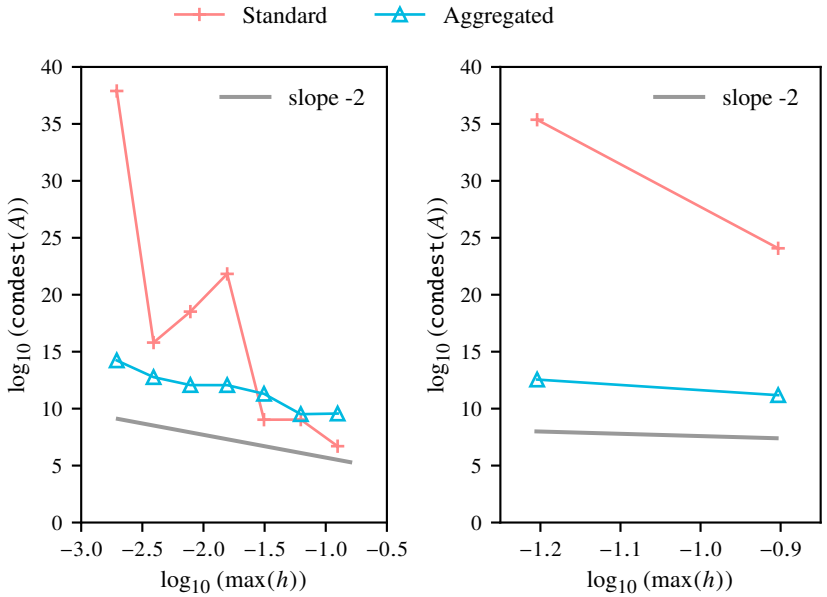

(a) 2D case. (b) 3D case.

FIG. 9. *Convergence test: Scaling of the condition number upon mesh refinement.*

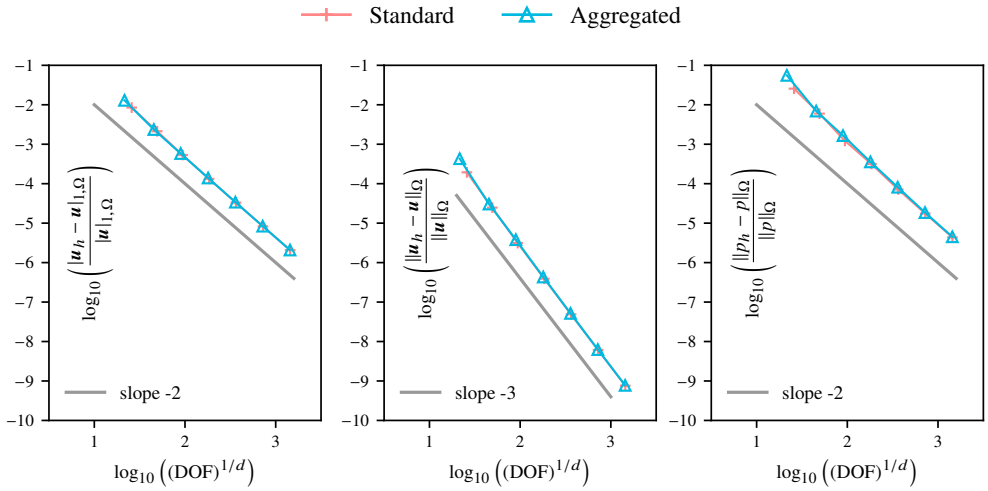

(a) Velocity H^1 semi-norm. (b) Velocity L^2 norm. (c) Pressure L^2 norm.

FIG. 10. *Convergence test: Convergence of the discretization error for the 2D case* ($d = 2$).

of the discretization error for the pressure field for the 2D and 3D cases, respectively. Since we consider second polynomial order for the velocities and first for the pressures, the optimal convergence orders are third order of convergence for the velocity error measured in the L^2 norm, second order for the velocity error in the H^1 seminorm,

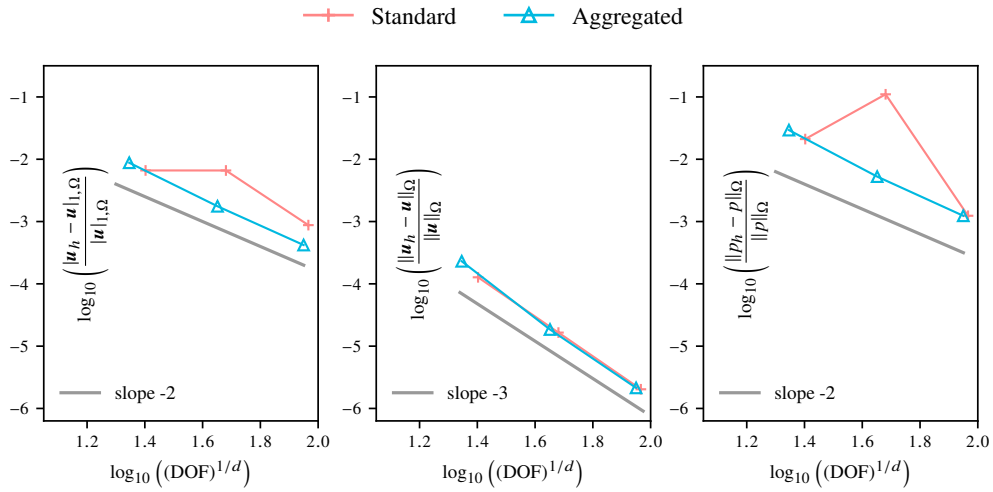

(a) Velocity H^1 semi-norm. (b) Velocity L^2 norm. (c) Pressure L^2 norm.

FIG. 11. *Convergence test: Convergence of the discretization error for the 3D case* ($d = 3$).

and second order for the pressure error in the L^2 norm. The plots show that the agFE spaces lead to these optimal FE convergence orders, which in turn confirms the analysis of section 6.4. Note that the standard (unaggregated) FE spaces lead to the optimal convergence orders in the 2D case (cf. Figure 10). However, it is clearly not the case in three dimensions (cf. Figure 11). The underlying linear systems are so ill-conditioned (reaching condition numbers up to 10^{35} as previously shown in Figure 9) that in general one cannot rely on the results computed by the linear solver using double precision floating point arithmetics. It can also be potentially caused by Nitsche's method losing stability in those cases in which cut cells are too thin, provided that the standard method selects the penalty of the Nitsche's method globally, instead of cellwise definitions that rely on local eigenvalue solvers. We have encountered some situations where the linear solver was indeed not able to provide an accurate solution for the reasons commented above; see, e.g., the red line in Figure 11(c). We note that the discretization errors of the standard and aggregated methods in Figures 10 and 11 are very close (for those cases in which the solver could provide a meaningful solution for the standard case). In this study, the manufactured solution is smooth, in particular on the boundaries. However, for flow problems with boundary layers, even though the same convergence rate is expected, there can potentially be an offset between the error plot of the standard and aggregate methods due to the fact that the aggregates increase the characteristic size (also reducing the number of DOFs) in the vicinity of the boundaries. In any case, h-adaptivity can naturally and elegantly solve this issue, which will be the object of future research.

7.3. Moving domain experiment. In the second numerical experiment, we study the robustness of the unfitted FE formulation with respect to the relative position between the problem geometry and the background mesh. To this end, we consider two geometries whose definition is parametrized by a scalar value ℓ (cf. Figure 12). The 2D geometry is a circular cavity, with radius $R = 0.225$ and

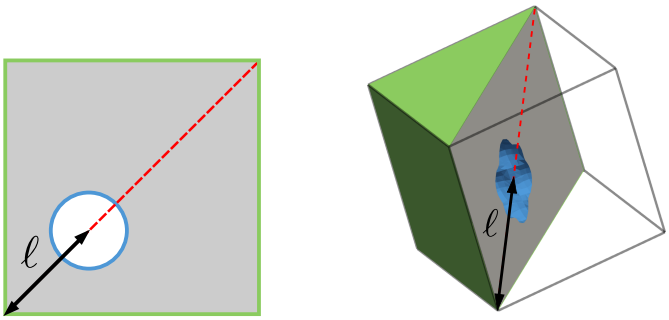

(a) 2D case. (b) 3D case (internal view).

FIG. 12. *Moving domain experiment: View of the problem geometries.*

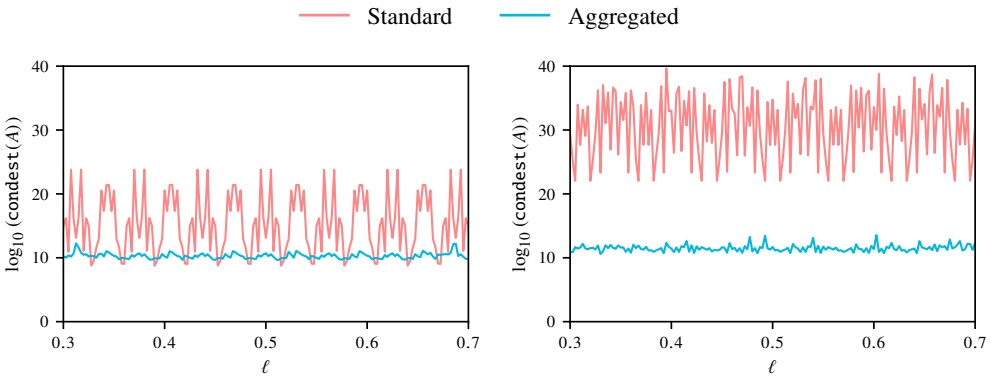

(a) 2D case. (b) 3D case.

FIG. 13. *Moving domain experiment: Condition number versus domain position.*

whose center is located at an arbitrary point on a diagonal of the unit square (cf. Figure 12(a)). The 3D domain is again a cavity defined using the popcorn flake geometry (cf. Figure 12(b)). In this case, we scale down the popcorn flake used in the convergence test (cf. section 7.2) by a factor of 0.5 and place it at an arbitrary point of the diagonal of the unit cube. In both cases, the position of the bodies is controlled by the value of the parameter ℓ (i.e., the distance between the center of the body and a selected vertex of the square/cube). As the value of ℓ varies, the objects move and their relative position with respect to the background mesh changes. In this process, arbitrary small cut cells can show up, leading to potential ill-conditioning problems. In this experiment, we consider a background mesh that discretizes the unit square/cube with 2^m elements per direction, where $m = 5$ for the 2D case and $m = 4$ for the 3D case.

Figure 13 shows the condition number estimate of the underlying linear systems versus ℓ. The plot is generated using a sample of 200 different values of ℓ. It is observed that the agFE spaces lead to condition numbers that are nearly independent of the value of ℓ, which shows that the agFEM is very robust regardless of how cells are cut. The benefit of using aggregation is clearly demonstrated here by observing the

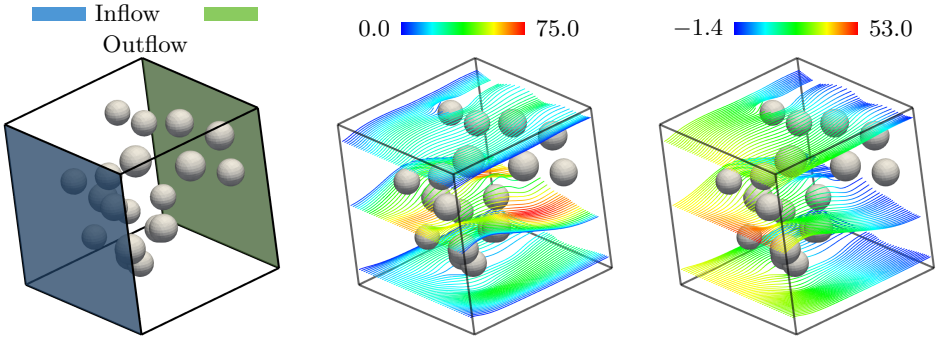

(a) Problem geometry. (b) Velocity (magnitude). (c) Pressure.

FIG. 14. *Complex 3D examples: Problem geometry and numerical solution for the Stokes flow around spherical obstacles (streamlines colored by velocity magnitude and pressure).*

results associated to the standard FE spaces. In that case, the condition numbers are very sensitive to the position of the geometry and reach very high values (condition number greater than 10^{35} in the 3D case).

7.4. Complex 3D examples. We conclude the numerical examples with the simulation of two complex geometries in order to show that the cell aggregation can be effectively used also in more complex settings. The first complex example is the simulation of a Stokes flow around a set of randomly spherical obstacles (see Figure 14). The (fluid) domain is the set difference of the unit cube $[0,1]^3$ and the spherical obstacles. We consider homogeneous Dirichlet conditions (no-slip conditions) in the surfaces of the spherical obstacles using Nitsche's method. The inflow boundary is the face $x = 0$ of the unit cube (see Figure 14(a)), where we impose a prescribed polynomial inflow velocity profile with value:

$$\boldsymbol{u} = (10y(y-1)z(z-1),\ 0,\ 0), \quad (x,y,z) \in \Gamma^{\text{in}} = \{0\} \times [0,1]^2.$$

The outflow boundary is the face $x = 1$ of the unit cube, where we impose homogeneous Neumann boundary conditions. We impose homogeneous Dirichlet conditions on the remaining faces of the cube. The problem is simulated using a background Cartesian mesh defined on the cube with 2^5 elements per direction. The obtained numerical solution is plotted in Figures 14(b) and 14(c). Note that the approximation of the velocities clearly conforms to the unfitted surfaces even though the interpolation is slightly coarsened near these surfaces by the cell aggregation.

The second complex example is a Stokes flow inside a spiral pipe (see Figure 15). The radius of the tubular cross section of the pipe is 0.1, whereas the radius of the spiral central axis is 0.875. We impose homogeneous Dirichlet conditions on the walls of the spiral. The inflow boundary is one of the two terminal cross sections of the pipe, i.e., the disk of center $C = (0, 0.875, 0.86)$ and radius $R = 0.1$ (see Figure 15(a)). On the inflow boundary we impose a parabolic velocity profile with value

$$\boldsymbol{u} = \left(10 - 10\frac{r^2}{R^2},\ 0,\ 0\right),$$

where $r \in [0, R]$ is the distance between a point x in the inflow boundary and the center C. Homogeneous Neumann boundary conditions are considered on the outflow

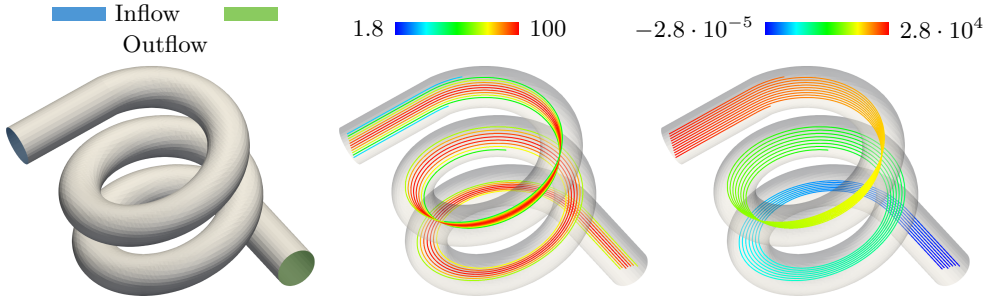

(a) Problem geometry. (b) Velocity (magnitude). (c) Pressure.

FIG. 15. *Complex 3D examples: Problem geometry and numerical solution for the Stokes flow in a spiral pipe (streamlines colored by velocity magnitude and pressure).*

boundary. Like in the previous example, the problem is simulated using a uniform Cartesian mesh of the unit cube with 2^5 elements at each direction. The results are shown in Figures 15(b) and 15(c). Note that even though it is a very challenging example for the cell-aggregation strategy because the surface to volume ratio is very high, the computed results reproduce a perfectly laminar velocity field that flows smoothly through the spiral pipe.

8. Conclusions. In this work, we have developed mixed agFEMs for the approximation of the Stokes problem on unfitted meshes. We have considered the standard extension operator for the definition of agFE spaces and a new one that relies on the extension of the serendipity component only (for hex meshes). A cell aggregation algorithm allows one to start with an FE mesh and create an aggregate partition with some desired properties. The agFE space is readily computed from a typical FE space plus simple cellwise constraints.

For the sake of conciseness, we have considered as a starting point mixed FE methods on body-fitted meshes with discontinuous pressure spaces on hexahedral meshes, considering both the standard and serendipity extension for the velocity field. We have performed an abstract stability analysis that relies on a set of assumptions, in order to prove a weak inf-sup condition for mixed agFE spaces. Such analysis shows the potential deficiency of the unfitted discrete inf-sup for such spaces. It allows us to identify a subset of aggregates/facets (*close* to the boundary), coined *improper* aggregates/facets; these subsets depend on the mixed agFE space being used.

Based on the abstract stability analysis, we have defined two different algorithms that satisfy the required assumption for having stability. The first algorithm relies on a standard velocity extension plus interior (residual-based) stabilization in improper aggregates and pressure jump stabilization on improper facets. The second algorithm relies on the serendipity extension for the velocity field components and pressure jump stabilization on improper facets. For these algorithms, a complete numerical analysis proves stability, a priori error estimates, and condition number bounds that are not affected by the small cut cell problem.

A complete set of numerical experiments bears out the numerical analysis. Finally, the mixed agFEM is applied to two problems with nontrivial geometries, viz., free flow in a medium with inclusions and confined flow in a spiral.

Acknowledgments. The authors want to thank the anonymous referees for their thorough revision of a previous version of this manuscript. Their suggestions and comments have substantially improved the paper. The authors thankfully acknowledge the computer resources at Marenostrum-IV and the technical support provided by the Barcelona Supercomputing Center (RES-ActivityID: FI-2018-1-0014).

REFERENCES

[1] N. Sukumar, N. Moës, B. Moran, and T. Belytschko, *Extended finite element method for three-dimensional crack modelling*, Internat. J. Numer. Methods Engrg., 48 (2000), pp. 1549–1570.
[2] S. Badia, F. Nobile, and C. Vergara, *Fluidstructure partitioned procedures based on Robin transmission conditions*, J. Comput. Phys., 227 (2008), pp. 7027–7051.
[3] H. Sauerland and T.-P. Fries, *The extended finite element method for two-phase and free-surface flows: A systematic study*, J. Comput. Phys., 230 (2011), pp. 3369–3390.
[4] E. Burman, D. Elfverson, P. Hansbo, M. Larson, and K. Larsson, *Shape optimization using the cut finite element method*, Comput. Methods Appl. Mech. Engrg., 328 (2018), pp. 242–261.
[5] M. Chiumenti, E. Neiva, E. Salsi, M. Cervera, S. Badia, J. Moya, Z. Chen, C. Lee, and C. Davies, *Numerical modelling and experimental validation in selective laser melting*, Additive Manufacturing, 18 (2017), pp. 171–185.
[6] C. Lang, A. Sharma, A. Doostan, and K. Maute, *Heaviside enriched extended stochastic FEM for problems with uncertain material interfaces*, Comput. Mech., 56 (2015), pp. 753–767.
[7] T. Belytschko, N. Mos, S. Usui, and C. Parimi, *Arbitrary discontinuities in finite elements*, Internat. J. Numer. Methods Engrg., 50 (2001), pp. 993–1013.
[8] E. Burman, S. Claus, P. Hansbo, M. G. Larson, and A. Massing, *CutFEM: Discretizing geometry and partial differential equations*, Internat. J. Numer. Methods Engrg., 104 (2015), pp. 472–501.
[9] D. Schillinger and M. Ruess, *The finite cell method: A review in the context of higher-order structural analysis of CAD and image-based geometric models*, Arch. Comput. Methods Engrg., 22 (2014), pp. 391–455.
[10] J. Parvizian, A. Dster, and E. Rank, *Finite cell method: h- and p-extension for embedded domain problems in solid mechanics*, Comput. Mech., 41 (2007), pp. 121–133.
[11] A. Düster, J. Parvizian, Z. Yang, and E. Rank, *The finite cell method for three-dimensional problems of solid mechanics*, Comput. Methods Appl. Mech. Engrg., 197 (2008), pp. 3768–3782.
[12] F. de Prenter, C. V. Verhoosel, G. J. van Zwieten, and E. H. van Brummelen, *Condition number analysis and preconditioning of the finite cell method*, Comput. Methods Appl. Mech. Engrg., 316 (2017), pp. 297–327.
[13] M. Dauge, A. Düster, and E. Rank, *Theoretical and numerical investigation of the finite cell method*, J. Sci. Comput., 65 (2015), pp. 1039–1064.
[14] S. Badia and F. Verdugo, *Robust and scalable domain decomposition solvers for unfitted finite element methods*, J. Comput. Appl. Math., 344 (2018), pp. 740–759.
[15] S. Badia, F. Verdugo, and A. F. Martin, *The aggregated unfitted finite element method for elliptic problems*, Comput. Methods Appl. Mech. Engrg., 336 (2018), pp. 533–553.
[16] S. Badia, A. F. Martn, and J. Principe, *FEMPAR: An object-oriented parallel finite element framework*, Arch. Comput. Methods Engrg., 25 (2018), pp. 195–271.
[17] FEMPAR, http://www.fempar.org/.
[18] E. Burman and P. Hansbo, *Fictitious domain finite element methods using cut elements:* II. *A stabilized Nitsche method*, Appl. Numer. Math., 62 (2012), pp. 328–341.
[19] E. Burman, *Ghost penalty*, C. R. Math., 348 (2010), pp. 1217–1220.
[20] J. Preuss, *Higher Order Unfitted Isoparametric Space-Time FEM on Moving Domains*, Master's thesis, University of Gottingen, 2018.
[21] C. Lehrenfeld and M. Olshanskii, *An Eulerian Finite Element Method for PDEs in Time-Dependent Domains*, arXiv:1803.01779, 2018.
[22] K. Höllig, U. Reif, and J. Wipper, *Weighted extended B-spline approximation of Dirichlet problems*, SIAM J. Numer. Anal., 39 (2001), pp. 442–462.
[23] T. Rüberg and F. Cirak, *Subdivision-stabilised immersed b-spline finite elements for moving boundary flows*, Comput. Methods Appl. Mech. Engrg., 209 (2012), pp. 266–283.
[24] T. Rüberg and F. Cirak, *A fixed-grid b-spline finite element technique for fluidstructure interaction*, Internat. J. Numer. Methods Fluids, 74 (2014), pp. 623–660.

[25] C. Helzel, M. Berger, and R. Leveque, *A high-resolution rotated grid method for conservation laws with embedded geometries*, SIAM J. Sci. Comput., 26 (2005), pp. 785–809.
[26] A. Johansson and M. G. Larson, *A high order discontinuous Galerkin Nitsche method for elliptic problems with fictitious boundary*, Numer. Math., 123 (2013), pp. 607–628.
[27] F. Kummer, *Extended discontinuous Galerkin methods for multiphase flows: The spatial discretization*, in Center for Turbulence Research Annual Research Briefs, 2013, pp. 319–333.
[28] E. Burman and P. Hansbo, *Fictitious domain methods using cut elements:* III. *A stabilized Nitsche method for Stokes' problem*, ESAIM Math. Model. Numer. Anal., 48 (2014), pp. 859–874.
[29] P. Hansbo, M. G. Larson, and S. Zahedi, *A cut finite element method for a {Stokes} interface problem*, Appl. Numer. Math., 85 (2014), pp. 90–114.
[30] L. Cattaneo, L. Formaggia, G. F. Iori, A. Scotti, and P. Zunino, *Stabilized extended finite elements for the approximation of saddle point problems with unfitted interfaces*, Calcolo, 52 (2015), pp. 123–152.
[31] J. Guzmán and M. Olshanskii, *Inf-sup stability of geometrically unfitted Stokes finite elements*, Math. Comp., 87 (2018), pp. 2091–2112.
[32] A. Massing, M. G. Larson, A. Logg, and M. E. Rognes, *A stabilized Nitsche fictitious domain method for the Stokes problem*, J. Sci. Comput., 61 (2014), pp. 604–628.
[33] C. Burstedde, L. C. Wilcox, and O. Ghattas, *p4est: Scalable algorithms for parallel adaptive mesh refinement on forests of octrees*, SIAM J. Sci. Comput., 33 (2011), pp. 1103–1133.
[34] H. Brezis, *Functional Analysis, Sobolev Spaces and Partial Differential Equations*, Springer, New York, 2010.
[35] A. Ern and J.-L. Guermond, *Theory and Practice of Finite Elements*, Springer, New York, 2004.
[36] D. N. Arnold and G. Awanou, *The serendipity family of finite elements*, Found. Comput. Math., 11 (2011), pp. 337–344.
[37] D. N. Arnold, D. Boffi, and R. S. Falk, *Approximation by quadrilateral finite elements*, Math. Comp., 71 (2002), pp. 909–922.
[38] S. C. Brenner and R. Scott, *The Mathematical Theory of Finite Element Methods*, Springer, New York, 2010.
[39] A. Johansson and M. G. Larson, *A high order discontinuous Galerkin Nitsche method for elliptic problems with fictitious boundary*, Numer. Math., 123 (2013), pp. 607–628.
[40] A. Hansbo and P. Hansbo, *An unfitted finite element method, based on Nitsche's method, for elliptic interface problems*, Comput. Methods Appl. Mech. Engrg., 191 (2002), pp. 5537–5552.
[41] H. Wu and Y. Xiao, *An Unfitted hp-Interface Penalty Finite Element Method for Elliptic Interface Problems*, arXiv:1007.2893, 2010.
[42] L. R. Scott and S. Zhang, *Finite element interpolation of nonsmooth functions satisfying boundary conditions*, Math. Comp., 54 (1990), pp. 483–493.
[43] R. Becker, *Mesh adaptation for Dirichlet flow control via Nitsche's method*, Commun. Numer. Methods Engrg., 18 (2002), pp. 669–680.
[44] J. Nitsche, *Über ein Variationsprinzip zur Lösung von Dirichlet-Problemen bei Verwendung von Teilräumen, die keinen Randbedingungen unterworfen sind*, Abh. Math. Semin. Univer. Hamb., 36 (1971), pp. 9–15.
[45] C. Bernardi, M. Costabel, M. Dauge, and V. Girault, *Continuity properties of the inf-sup constant for the divergence*, SIAM J. Math. Anal., 48 (2016), pp. 1250–1271.
[46] H. C. Elman, D. J. Silvester, and A. J. Wathen, *Finite Elements and Fast Iterative Solvers: With Applications in Incompressible Fluid Dynamics*, Oxford University Press, New York, 2005.
[47] Intel MKL PARDISO–Parallel Direct Sparse Solver Interface, https://software.intel.com/en-us/articles/intel-mkl-pardiso.
[48] QHULL, http://www.qhull.org/.
[49] C. B. Barber, D. P. Dobkin, and H. Huhdanpaa, *The Quickhull algorithm for convex hulls*, ACM Trans. Math. Software, 22 (1996), pp. 469–483.